

Nonparametric Bayes Differential Analysis for Dependent Multigroup Data with Application to DNA Methylation Analyses in Cancer

Chiyu Gu*

Department of Statistics, University of Missouri
and

Veerabhadran Baladandayuthapani

Department of Biostatistics, The University of Texas M.D. Anderson Cancer Center
and

Subharup Guha

Department of Biostatistics, University of Florida

*The first author is currently working with Bayer Crop Science, and the second author is at the Department of Biostatistics, University of Michigan. This work was supported by the National Science Foundation under Award DMS-1854003 to SG and Award DMS-1463233 to VB, and by the National Institutes of Health under Grant R01 CA160736 to VB. The work was partially supported by the National Science Foundation under Grant DMS-1127914 to the Statistical and Applied Mathematical Sciences Institute, RTP, North Carolina.

Abstract

Modern cancer genomics datasets involve widely varying sizes and scales, measurement variables, and correlation structures. A fundamental analytical goal in these high-throughput studies is the development of general statistical techniques that can cleanly sift the signal from noise in identifying disease-specific genomic signatures across a set of experimental or biological conditions. We propose *BayesDiff*, a nonparametric Bayesian approach based on a novel class of first order mixture models, called the Sticky Poisson-Dirichlet process or multicuisine restaurant franchise. The BayesDiff methodology flexibly utilizes information from all the measurements and adaptively accommodates any serial dependence in the data, accounting for the inter-probe distances, to perform simultaneous inferences on the variables. The technique is applied to analyze a DNA methylation gastrointestinal (GI) cancer dataset, which displays both serial correlations and complex interaction patterns. Our analyses and results both support and complement known aspects of DNA methylation and gene association in upper GI cancers. In simulation studies, we demonstrate the effectiveness of the BayesDiff procedure relative to existing techniques for differential DNA methylation.

Keywords: Genomic signature; First order models; Mixture models; Multicuisine restaurant franchise; Sticky Poisson-Dirichlet process

1 Introduction

Recent advances in array-based and next-generation sequencing (NGS) technologies have revolutionized biomedical research, especially in cancer. The rapid decline in the cost of genome technologies enables the measurement of genomic activity at a very detailed resolution and provides genome-wide information at the transcriptomic (e.g., gene/mRNA expression), genomic (e.g., copy number variation), epigenomic (e.g., methylation), and proteomic levels on matched patient or tissue samples (Hamid et al. 2009). These datasets involve intrinsically different sizes and scales of high throughput data, providing genome-wide, high resolution information about the biology of cancer.

A common goal is the identification of differential genomic signatures between samples corresponding to different treatments or biological conditions, e.g., treatment arms, response to adjuvant chemotherapy, tumor subtypes, or cancer stages. The analytic challenges include the high dimensionality of genomic markers such as genes and probes, usually in the hundreds of thousands, and the relatively small number of patient samples, usually no more than a few hundred. This “small n , large p ” problem results in unstable inferences due to collinearity. There also exist complex interaction patterns, such as signaling or functional pathway-based interactions for gene or protein expression data, and genomic or chromosomal location-based serial correlation for high-throughput sequencing data. These interaction patterns can significantly influence the reliable detection of differential genomic signatures.

Differential DNA Methylation in Gastrointestinal Cancer

DNA methylation is a vitally important epigenetic mechanism that occurs by the addition of a methyl (CH_3) group to DNA, resulting in the modification of the gene functions. This typically occurs at specific genomic locations called cytosine-phosphate-guanine (CpG) sites. Alterations in DNA methylation, e.g., hypomethylation of oncogenes and hypermethylation of tumor suppressor genes (Feinberg & Tycko (2004)), are often associated with the development and progression of cancer. It was previously believed that these alterations almost exclusively occur in specific promoter regions known as CpG islands, which are chromosomal regions with a high frequency of CpG sites. However, with the advent of high-throughput technologies, it has been shown that a significant proportion of methylation alterations in cancer do not occur in either promoters or CpG islands (Irizarry et al. 2009), prompting higher resolution, epigenome-wide investigations.

Gastrointestinal (GI) cancer, the most common form of cancer in the U.S. (Siegel et al. 2017), refers to malignant conditions affecting the digestive system. This includes cancers of the esophagus, gallbladder, liver, pancreas, stomach, small intestine, bowel and anus. In the motivating application, we focused on four types of GI cancers related to the upper digestive tract: stomach adenocarcinoma (STAD), liver hepatocellular carcinoma (LIHC), esophageal carcinoma (ESCA) and pancreatic adenocarcinoma (PAAD). Epigenetic alterations are usually observed in these types of GI cancer (Vedeld et al. 2017). For example, infections involving *Helicobacter pylori* and Epstein-Barr virus, two major risk factors for stomach cancer, are associated with increased levels of promoter DNA methylation (Maekita et al. 2006, Graham 2015, Network et al. 2014). Hypermethylation of the gene *CDKN2A* is often present in large contiguous fields of ESCA samples (Eads et al. 2000). Molecular characterization of the cancer types, facilitated by the identification of differentially methylated sites, is therefore key to gaining a better understanding of GI cancer.

We analyze methylation profiles publicly available from The Cancer Genome Atlas (TCGA) project, with a total of 1,224 tumor samples belonging to the four GI cancer types. For 485,577 probes, DNA methylation levels ranging from 0 (no methylation) to 1 (full methylation) were measured using the Illumina Human Methylation 450 platform, with each probe mapped to one CpG site. Figure 1(a) displays the methylation levels for CpG sites near TP53, a tumor suppressor gene located on chromosome 17. The four sets of colors and shapes of the points represent the four GI cancers. Although differential methylation is clearly visible in some CpG sites, the differences are generally subtle and hard to distinguish, demonstrating the need for sophisticated statistical analyses. A common feature of DNA methylation data is the correlation between the methylation status of nearby CpG sites (Eckhardt et al. 2006, Irizarry et al. 2008, Leek et al. 2010). This can be seen in Figure 1(b), which reveals fairly high first order autocorrelations for most of the

samples, along with highly significant tests for serial correlations. Furthermore, the high variability of the inter-probe spacings in Figure 1(a) suggests that distance-based dependencies would provide a better fit to the data.

Existing statistical approaches Numerous frequentist and Bayesian methods have been developed for differential DNA methylation. Existing approaches can be broadly classified into four categories: (i) *Testing-based methods*, such as Illumina Methylation Analyzer (IMA) (Wang et al. 2012), City of Hope CpG Island Analysis Pipeline (COHCAP) (Warden et al. 2013), and BSmooth (Hansen et al. 2012). These methods rely on two-sample or multiple-sample tests for the difference in means at each CpG site. (ii) *Regression based models*, such as MethyKit (Akalın et al. 2012), bump hunting (Jaffe et al. 2012), Biseq (Hebestreit et al. 2013), and RADMeth (Dolzhenko & Smith 2014). After applying smoothing or other adjustments, these methods fit individual regression models for each CpG site and test for significance. (iii) *Beta-binomial model-based methods*, such as MOABS (Sun et al. 2014), DSS (Feng et al. 2014), and methylSig (Park et al. 2014). These methods fit separate models for each CpG site based on the beta-binomial distribution and detect differential CpG sites via estimated model parameters. (iv) *Hidden Markov models (HMMs)*, such as MethPipe (Song et al. 2013), Bisulfighter (Saito et al. 2014), and HMM-DM (Yu & Sun 2016). These methods rely on HMMs to model the methylation data for the entire genome and detect differentially methylated sites based on the inferred hidden states.

The aforementioned methods, although effective, have some important shortcomings. For instance, most methods ignore the strong correlations between neighboring CpG sites. The non-HMM methods fit separate models to each CpG site, thereby reducing the detection power due to the small sample sizes. The beta-binomial, HMM, and most of the testing-based methods are able to accommodate only two treatments or groups. To handle multiple treatments, they typically resort to low-power multiple comparison adjustments.

Among methods capable of accounting for serial dependence (e.g., HMMs), a common drawback is that they fail to adjust for the widely varying distances between the CpG sites. That is, irrespective of the distances between neighboring sites, these methods assume that the inter-site dependencies are uniform. However, empirical evidence (e.g., Figure 1) strongly suggests that the dependencies decrease with increasing distance. The few methods that do account for inter-site distances (e.g., Hansen et al. 2012, Jaffe et al. 2012, Hebestreit et al. 2013) often rely on ad hoc procedures to determine their tuning parameters, such as bandwidths, and do not adequately adjust for the unique characteristics of the datasets.

Furthermore, most of the aforementioned methods have been specially developed for a particular data type (e.g., either DNA methylation arrays or bisulfite sequencing data), and are not applicable to differently sized and scaled data (e.g., gene or mRNA expression data).

This paper proposes general and flexible methodology for differential analysis, referred to as *BayesDiff*. Rather than fitting a separate model for each genomic locus or probe, BayesDiff relies on a global framework for simultaneous inferences on the probes and is capable of adapting to the distinctive features of omics datasets. A set of probe-specific differential state variables delineates the genomic signature of the disease, and is a deterministic function of a set of latent random effects vectors. To diminish collinearity effects and achieve dimension reduction in the large number of probes, we allocate the probes to a smaller, unknown number of latent clusters based on the similarities of their multivariate random effects. We devise a novel extension of Poisson Dirichlet processes (PDPs) (Perman et al. 1992) called the *Sticky PDP* (or, equivalently, the *multicuisine restaurant franchise*) for modeling the probe-cluster allocation mechanism. In addition to accounting for long range biological interactions between non-adjacent probes, the nonparametric stochastic process accommodates distance-based serial dependencies between the probes. The correlation strength is determined by a univariate dependence parameter that can be learned from the data. For example, the estimated dependence parameter would be zero in datasets that do not support inter-probe serial dependence. Furthermore, the model permits the data to direct the choice between PDPs, and their special case, Dirichlet processes, in finding the best-fitting allocation scheme separately for non-differential and non-differential probes. The methodology is applicable to differential analysis in genomic, epigenomic, transcriptomic, and proteomic datasets.

We implement a fully Bayesian inferential procedure using a Markov chain Monte Carlo (MCMC) algorithm specifically developed for posterior inferences in Sticky PDPs. The MCMC strategy is scalable to the ubiquitous big datasets in cancer research. Bayesian false discovery rate (FDR) control is implemented for multiplicity adjustment. Simulation results show that our approach significantly outperforms existing methods for multigroup comparisons in datasets with or without serial correlation. For the motivating GI cancer data, in addition to confirming known features of DNA methylation and gene associations with cancer, the analysis revealed interesting facts about the biological mechanisms of the four cancer types.

The rest of the paper is organized as follows. Section 2 describes the BayesDiff model. Section 2.1 invents a new nonparametric Bayesian stochastic process, the Sticky Poisson-Dirichlet process, for differential analysis. The general form of the Sticky PDP and its connection to existing Bayesian mixture models are examined in Section 2.2. Section 3 outlines a computationally efficient posterior inference procedure for detecting differential probes. For different noise and correlation levels,

Section 4 uses artificial datasets to evaluate the accuracy of BayesDiff in detecting disease genomic signatures and makes comparisons with established techniques. The motivating GI dataset is analyzed using the BayesDiff procedure in Section 5. Conclusions and future related work are discussed in Section 6.

2 The BayesDiff Model

Assume that we have continuous, proportion, or count measurements on p biomarkers such as genes or CpG sites (“probes”), and on n matched patient or tissue samples (“individuals”), with p being much larger than n . The data are arranged in an $n \times p$ matrix, $\mathbf{X} = ((x_{ij}))$ for individuals i and probes j , and the probes are sequentially indexed by their genomic locations. The distances between the adjacent probes are denoted by e_1, \dots, e_{p-1} , and usually have a significant amount of variability. In the GI cancer dataset, the DNA methylation levels belong to the interval $[0, 1]$, and the inter-probe distances range from 2 base pairs to more than 1,141K base pairs.

Each individual i is associated with an experimental or biological condition (“treatment”), and the treatment label t_i takes values in the set $\{1, \dots, T\}$ for some $T \geq 2$. In the motivating application, $T = 4$, because we consider four GI cancer types. We make a suitably chosen platform-specific transformation $z(\cdot)$, and define the transformed measurement, $z_{ij} = z(x_{ij})$. For count data $x \in \mathbb{N}$, an appropriate transformation could be $z(x) = \log(1 + x)$. For proportion data $0 < x < 1$, the logit function, $z(x) = \log(x/(1 - x))$ may be appropriate. For continuous data $x \in \mathbb{R}$, we could simply choose the identity transformation. It is assumed that

$$z_{ij} = z(x_{ij}) \sim N(\xi_i + \chi_j + \theta_{t_i j}, \sigma^2) \quad (1)$$

where ξ_i represents the i th subject’s random effect, χ_j represents the j th probe’s random effect, and $\theta_{t_i j}$ is the unknown treatment t –probe j interaction.

Depending on the specifics of the application, an appropriate model is assumed for the subject-specific parameters ξ_1, \dots, ξ_n . For example, we may assume that $\xi_i \stackrel{iid}{\sim} N(0, \tau_\epsilon^2)$. In some applications, it is more reasonable to assume non-zero means: $\xi_i \stackrel{iid}{\sim} N(b_i, \tau_\epsilon^2)$, where b_i denotes a known individual-specific constant. Examples include RNASeq differential analysis, where the b_i ’s may represent the lane or batch effects available from previous studies. Similarly, an appropriate model is assumed for the probe-specific parameters χ_1, \dots, χ_p . Examples include i.i.d. zero-mean normal distributions, and finite mixture models or HMMs with a finite number of latent states and state-specific normal distributions. Inverse-Gamma priors are assigned to the variance parameters, σ^2 and τ_ϵ^2 .

Our primary goal is the detection of differential probes. From the perspective of the model, the differential probes j are those probes whose treatment-specific effects $\boldsymbol{\theta}_j = (\theta_{1j}, \dots, \theta_{Tj})'$ are not all identical. Inference therefore focuses on the p vectors of treatment-specific random effects. We define a binary *differential state variable*, s_j , with the value $s_j = 1$ indicating that probe j is not differential, and value $s_j = 2$ indicating that it is differential. That is,

$$s_j = \begin{cases} 1 & \text{if } \theta_{1j} = \theta_{2j} = \dots = \theta_{Tj}, \\ 2 & \text{otherwise,} \end{cases} \quad (2)$$

for $j = 1, \dots, p$. The disease genomic signature consists of the probes with state $s_j = 2$. The key parameters of interest are therefore the differential state variables, s_1, \dots, s_p . We assume flexible Bayesian nonparametric models for random effects $\boldsymbol{\theta}_1, \dots, \boldsymbol{\theta}_p$, as discussed below.

Modeling the probe clusters

In addition to high-dimensionality, the analytical challenges posed by cancer datasets include pervasive collinearity caused by dependencies between physically proximal probes and dependencies due to longer range biological interactions between non-adjacent probes, e.g., through signaling or functional pathway-based interactions. Collinearity is known to cause inaccuracies in estimation and uncertainty quantification. To mitigate the effects of collinearity and extract information from the large number of probes through dimension reduction, we allocate the p probes to a much smaller number, q , of latent clusters based on the similarities of the probe-specific random effects $\boldsymbol{\theta}_j$. We favor clustering to unsupervised dimension reduction methods such as principal components analysis (PCA). Specifically, because each principal component is a linear combination functions of all p biomarkers, PCA achieves dimension reduction but not feature (i.e. probe or biomarker) selection. In contrast, our findings have direct biological interpretations in terms of potentially relevant biomarkers and are directly applicable to the problem of differential analysis.

Suppose that an *allocation variable*, c_j , assigns probe j to one of q latent clusters, where q is unknown. The event $[c_j = k]$ implies that the j^{th} probe belongs to the k^{th} cluster, $k = 1, \dots, q$. The q clusters are assumed to be associated with *latent vectors*, $\boldsymbol{\lambda}_1, \dots, \boldsymbol{\lambda}_q$, each length T . The probe-specific random effects and cluster-specific latent vectors have the relation

$$\boldsymbol{\theta}_j = \boldsymbol{\lambda}_k \quad \text{if } c_j = k. \quad (3)$$

In other words, all probes assigned to a cluster have identical random effects equal to that cluster's

latent vector. The probes' differential state variables, defined in equation (2), are then attributes of their parent clusters, and the clusters as a whole are either differential or non-differential. The condition $\theta_{1j} = \theta_{2j} = \dots = \theta_{Tj}$ in equation (2) is equivalent to the condition $\lambda_{1k} = \lambda_{2k} = \dots = \lambda_{Tk}$ if probe j belongs to cluster k (i.e., if $c_j = k$). We represent the set of *differential clusters* as

$$\mathcal{D} = \left\{ k : \lambda_{tk} \neq \lambda_{t'k}, \text{ for some } t \neq t', k = 1, \dots, q \right\} \quad (4)$$

Existing mixture models for allocations Bayesian infinite mixture models are a natural choice for allocating p probes to a smaller, unknown number of latent clusters based on the similarities of their random effects. Dirichlet processes (Ferguson 1973a) are the most frequently used infinite mixture models; see Müller & Mitra (2013, chap. 4) for a comprehensive review. The use of Dirichlet processes to achieve dimension reduction in massive datasets has precedence in the literature (see Medvedovic et al. 2004, Kim et al. 2006, Dunson et al. 2008, Dunson & Park 2008, Guha & Baladandayuthapani 2016). Lijoi, Mena & Prünster (2007a) advocated the use of Gibbs-type priors (Gnedin & Pitman 2005, Lijoi, Mena & Prünster 2007b) for accommodating more flexible clustering mechanisms. In particular, (Lijoi et al. 2007a) demonstrated the utility of Poisson-Dirichlet processes (PDPs) in genomic applications. Guha & Baladandayuthapani (2016) introduced VariScan, a technique that utilizes standard PDPs and Dirichlet processes for clustering, variable selection, and prediction in high-dimensional regression problems. They also demonstrated that PDPs are overwhelmingly favored to Dirichlet processes in gene expression datasets with negligible serial correlation.

The two-parameter PDP (Perman et al. 1992) relies on a discount parameter $d \in [0, 1)$, positive mass parameter α , and T -variate base distribution W , and is denoted by $\mathcal{W}(d, \alpha, W)$. The value $d = 0$ yields a Dirichlet process with mass parameter α and base distribution W . Suppose the sequence of random effects $\theta_1, \dots, \theta_p$ are distributed as $\mathcal{W}(d, \alpha, W)$. The *stick-breaking representation* of the PDP is $\theta_j \stackrel{iid}{\sim} \mathcal{P}$, where random distribution \mathcal{P} is the discrete mixture $\sum_{v=1}^{\infty} \pi_v \delta_{\phi_v}$, with δ_{ϕ_v} denoting a point mass located at the atom $\phi_v \stackrel{iid}{\sim} W$. The random stick-breaking probabilities have the form: $\pi_1 = V_1$ and $\pi_h = V_h \prod_{v=1}^{h-1} (1 - V_v)$ for $h > 1$, where $V_h \stackrel{indep}{\sim} \text{beta}(1 - d, \alpha + hd)$.

Limitations of existing approaches Although the aforementioned mixture models achieve dimension reduction in the large number of probes and account for long range biological interactions between non-adjacent probes, a potential drawback is their implicit assumption of apriori probe exchangeability. Consequently, these techniques, including the VariScan method of Guha & Baladandayuthapani (2016), are unable to account for serial correlation in the probes. This is a serious disadvantage in differential analysis applications. Infinite HMMs, such as the hierarchi-

cal Dirichlet process hidden Markov model (HDP-HMM) (Teh et al. 2006) and Sticky HDP-HMM (Fox et al. 2011) may be utilized to fill this gap. In these models, each probe j has an associated *group* depending on the preceding probe’s random effect, θ_{j-1} . The group, in turn, determines the distribution of random effect θ_j , inducing first order dependence between the random effects.

Infinite HMMs are a step in the right direction, but these models have some undesirable features for differential analysis in cancer data. *First*, the degree of first order dependence is uniform irrespective of the inter-probe distances. This is unrealistic in epigenomic datasets where the correlation between adjacent probes typically decreases with the distance (Hansen et al. 2012, Jaffe et al. 2012, Hebestreit et al. 2013). *Second*, the set of distinct treatment-probe interactions is potentially infinite and has a bijective mapping with the set of groups, which is therefore also infinite. In contrast, using first order Bayesian mixture models, an ad hoc exploratory analysis of some samples from the GI cancer dataset reveals that the serial correlation in the treatment-probe effects is weaker than the serial dependence between the differential state variables defined in equation (2). Although there may not be a biological explanation for this observation, it makes sense from a statistical perspective, because the differential states are binary functions of the treatment-probe interactions. The differential states are therefore more sensitive in detecting first order dependence even when the higher-dimensional (and noisier) treatment-probe interactions show weak or no correlation. This suggests that a hypothetical two-group Markov model, rather than an infinite-group Markov model such as HDP-HMM or Sticky HDP-HMM, would provide a better fit for the data. *Third*, the range of allocation patterns supported by infinite HMMs is relatively limited. In particular, patterns such as power law decays in the cluster sizes and large numbers of small-sized clusters, a common feature of cancer datasets, are assigned relatively small prior probabilities by infinite HMMs.

For these reasons, we propose a novel extension of PDPs called the Sticky PDP, capable of accommodating distance-based serial dependencies between the probes and allowing far fewer groups than random effects clusters. Informally, a Sticky PDP is a cohort of regular PDPs that generates the probe-specific random effects, $\theta_1, \dots, \theta_p$, by switching the generative PDPs at random locations along the probe sequence. The well-known Chinese restaurant franchise (CRF) metaphor for HDP-HMMs and Sticky HDP-HMMs (e.g., Fox et al. 2011) can be generalized to the *multicuisine restaurant franchise* (MRF) to provide an equivalent representation of Sticky PDPs. Through the MRF representation, Section 2.1 fosters an appropriate framework for differential analysis in potentially dependent data. Later, the general form of the Sticky PDP is presented in Section 2.2.

2.1 A Two-restaurant, Two-cuisine Franchise for Differential Analysis

Suppose that a franchise has two restaurants, labeled 1 and 2. Each restaurant consists of two sections, with each section exclusively serving a particular cuisine consisting of an infinite number of dishes. Section 1 in both restaurants exclusively caters to cuisine 1, whereas section 2 exclusively caters to cuisine 2 in both the restaurants. Restaurant 1 specializes in cuisine 1, and consequently, that cuisine is much more popular with its patrons. Similarly, restaurant 2 specializes in cuisine 2. A *cuisine menu* is an inventory of available dishes belonging to a cuisine and is identical at the two restaurants. However, the relative popularity of the menu items are different for the restaurants.

A succession of customers, representing the p probes, arrive at the franchise. The waiting times between successive customers, e_1, \dots, e_{p-1} , represent the inter-probe distances in the application. Each of the four restaurant sections has an infinite number of tables at which customers could potentially sit. A customer who selects a particular section (i.e. cuisine) in a restaurant may either sit at one of the tables already occupied by previous customers in that section, or the customer may choose to sit at a new, unoccupied table. All customers who are seated at a table in a restaurant section must be served the same dish, chosen from the cuisine menu by the first customer who sat at that table. Multiple tables within a section are allowed to serve the same dish.

The dishes that the franchise customers eat represent the T -variate probe-specific random effects in the application. Cuisine 1 represents the *non-differential state*, and thus, the cuisine 1 dishes are random effects of length T with all equal elements. Cuisine 2 represents the *differential state* and the cuisine 2 dishes are T -variate random vectors with at least two unequal treatment effects. Thus, cuisines 1 and 2 are uniquely identified by their dishes.

By design, if a customer has eaten a dish belonging to cuisine 1 (2), the next customer is more likely to visit restaurant 1 (2), where that cuisine is more popular. In this manner, a customer is more likely to select the same cuisine as the previous customer. Applied to differential analysis, this feature accounts for long runs of differential or non-differential states of the probes. However, a customer's influence on the next customer diminishes as the time interval separating the two customers increases. That is, the differential status of any two adjacent probes become statistically independent in the limit as the inter-probe distance grows. In addition to achieving dimension reduction in the large number of probes and accounting for long range interactions between non-adjacent probes, the following Sticky PDP provides a framework for modeling the serial dependence of the differential status as a decreasing function of inter-probe distance. Further details are provided below.

2.1.1 Cuisine menus

Cuisine 1 menu. The available dishes in cuisine 1, characterizing random vectors for which all T elements are equal, are modeled by *menu distribution* W_1 having the following special structure. With $\mathbf{1}_T$ denoting the column vector of T ones,

$$\begin{aligned} W_1 &\stackrel{d}{=} \psi \mathbf{1}_T, \quad \text{where } \psi \in \mathcal{R} \text{ with} \\ \psi &\sim G \quad \text{and} \\ G &\sim \mathcal{DP}(\beta, G_0). \end{aligned} \tag{5}$$

The last symbol denotes a Dirichlet process prior with positive mass parameter β and univariate base distribution, $G_0 = N(\mu_G, \tau_G^2)$. The stick-breaking representation of the Dirichlet process implies that random distribution G is almost surely discrete, and has the mixture distribution

$$G \stackrel{d}{=} \sum_{v=1}^{\infty} \varpi_v \delta_{\zeta_v}, \quad \text{where } \sum_{v=1}^{\infty} \varpi_v = 1 \text{ and } \zeta_v \stackrel{iid}{\sim} G_0. \tag{6}$$

The precise form of the random probabilities, ϖ_v , which depend on mass parameter β , was derived in Sethuraman (1994); see also Ishwaran & James (2003) and Lijoi & Prünster (2010). For natural numbers \mathcal{N} , the set $\mathcal{S}_1 = \{\zeta_v \mathbf{1}_T : v \in \mathcal{N}\}$ represents the list of available cuisine 1 dishes, and is the support of distribution W_1 . The continuity of base distribution G_0 guarantees that all dishes are unique. The fact that distribution G is discrete has useful consequences in this application: (a) cuisine 1 consists of a countably infinite set, rather than a continuous spectrum, of dishes, and (b) tables belonging to different restaurants could possibly serve the same cuisine 1 dish.

Cuisine 2 menu. The cuisine dishes characterize T -variate random vectors with at least two unequal elements. The menu is modeled by a distribution, W_2 , satisfying two conditions: (i) for similar reasons as for the cuisine 1 menu, W_2 is a countably infinite distribution, and (ii) each atom of W_2 has at least two unequal elements. For every $\phi = (\phi_1, \dots, \phi_T)' \in \mathcal{R}^T$, a probability mass function satisfying these two conditions can be constructed as follows:

$$W_2(\phi) = \begin{cases} \prod_{t=1}^T G(\phi_t) / (1 - \sum_{v=1}^{\infty} \varpi_v^T) & \text{if } \phi_t \neq \phi_{t'} \text{ for some } t \neq t', \\ 0 & \text{otherwise.} \end{cases} \tag{7}$$

where $G(\phi)$ denotes the mass function of distribution G , defined in equation (6) and evaluated at $\phi \in \mathcal{R}$. Then, as required, the menu distribution W_2 is discrete and has the countable support,

$$\mathcal{S}_2 = \{(\zeta_{v_1}, \dots, \zeta_{v_T})' : \zeta_{v_t} \neq \zeta_{v_{t'}} \text{ for some integers } v_t \neq v_{t'}, \text{ where } (v_1, \dots, v_T) \in \mathcal{N}^T\}.$$

We observe that the differential and non-differential states communicate through distribution G . When the number of treatments, T , is large, the discreteness of distribution G causes dimension reduction in the T -variate differential state atoms by allowing ties between the atom elements, and resulting in a relatively small number of unique elements within each atom of length T . This model feature facilitates computational savings for the inferential procedure when T is large.

2.1.2 Customer 1

Suppose that the first franchise customer, arriving at time 0, selects restaurant 1 with positive probability ρ_1 and selects restaurant 2 with positive probability $\rho_2 = 1 - \rho_1$. For reasons that will soon be clear, we refer to ρ_2 as the *baseline differential proportion* and ρ_1 as the *baseline non-differential proportion*. Typically, the differential state is less frequent than the non-differential state; so $\rho_2 < \rho_1$ (i.e. $\rho_2 < 1/2$). Let g_1 be the restaurant chosen by customer 1.

Choice of cuisine s_1 Next, customer 1 proceeds to enter a cuisine-section within restaurant g_1 . Recall that each restaurant specializes in the cuisine having the same label, and the specialty cuisine is more popular there. In differential analysis, this is guaranteed by the following assumption. More generally, let the restaurant chosen by customer j (where $j = 1$ for the first customer) be denoted by g_j . Within restaurant g_j , assume that customer j selects cuisine 1 with probability

$$\mathcal{Q}_{g_j}(1) = \begin{cases} \rho_1 + \rho_2\gamma & \text{if } g_j = 1, \\ \rho_1 - \rho_1\gamma & \text{if } g_j = 2, \end{cases} \quad (8)$$

for a *speciality-cuisine popularity parameter*, $\gamma \in (0, 1]$, quantifying the degree to which a restaurant's patrons tend to favor its namesake cuisine. Expression (8) implies that $\mathcal{Q}_{g_j}(2) = 1 - \mathcal{Q}_{g_j}(1)$ is the probability of a customer choosing cuisine 2 in restaurant g_j . Let the cuisine (i.e. restaurant section) chosen by customer j be generically denoted by s_j .

Choice of table v_1 and dish θ_1 We focus again on customer 1. Since the table identifiers are arbitrary, among the infinite tables belonging to section s_1 of restaurant g_1 , we assume without loss of generality that customer 1 sits at table $v_1 = 1$, and that the tables in each restaurant section have consecutive labels as they are progressively occupied by incoming patrons. Next, customer 1

randomly orders a dish from menu distribution W_{s_1} . That is, $\theta_1 \mid s_1 \sim W_{s_1}$. In differential analysis, the dish represents random effect θ_1 of the first probe.

2.1.3 Subsequent franchise customers

Customer j , where $j > 1$. Unlike customer 1, the *restaurant* choices of all subsequent customers are influenced by the *cuisine* of the customer immediately preceding them and by the waiting time between successive customers. When $j > 1$, suppose customer j arrives at the franchise after a waiting time of e_{j-1} following customer $(j-1)$'s arrival. For a non-negative **dependence parameter** η , the waiting time e_{j-1} is first transformed to an **affinity** between customer $(j-1)$ and customer j :

$$r_j = \exp(-e_{j-1}/\eta), \quad j > 1, \quad (9)$$

which belongs to the interval $[0, 1]$. If $\eta = 0$, affinity r_j is defined as 0 irrespective of waiting time.

We may assume, without loss of generality, that the waiting times e_1, \dots, e_{p-1} are scaled so that their total equals 1. For example, if the probes in differential analysis represent biomarkers on a chromosome, and if the first probe is located near the chromosomal edge, then after scaling, the chromosome has approximately unit standardized length.

Choice of restaurant g_j For an affinity r_j between customers $(j-1)$ and j , and given that customer $(j-1)$ had selected cuisine s_{j-1} , the conditional probability that customer j selects restaurant 1 is assumed to be

$$\mathcal{F}_j(1) \stackrel{\text{def}}{=} P(g_j = 1 \mid s_{j-1}) = \begin{cases} \rho_1 + \rho_2 r_j / \gamma & \text{if } s_{j-1} = 1, \\ \rho_1 - \rho_1 r_j / \gamma & \text{if } s_{j-1} = 2. \end{cases} \quad (10)$$

The probability that customer j selects restaurant 2 is $\mathcal{F}_j(2) = 1 - \mathcal{F}_j(1)$. In other words, $g_j \mid s_{j-1} \sim \mathcal{F}_j$.

The idea is illustrated in the top panel of Figure 2, where customer j chooses restaurant 1 with probability $\mathcal{F}_j(1)$ and chooses restaurant 2 with probability $\mathcal{F}_j(2)$. As seen from definition (10), if $\eta > 0$, these probabilities depend on the cuisine section s_{j-1} of the previous customer and on the between-customer waiting time, e_{j-1} . If $\eta = 0$, on the other hand, the restaurant choices of the customers are independent of one another, and $\mathcal{F}_j(g) = \rho_g$ for $g = 1, 2$.

It can be easily verified that \mathcal{F}_j is a probability mass function if and only if $r_j/\gamma < 1$. Since the standardized waiting times are bounded above by 1, a globally sufficient condition is then

$\eta < -1/\log \gamma$. We therefore assume a mixture prior having the general form:

$$\eta \mid \gamma \sim \frac{1}{2}\delta_0 + \frac{1}{2}\mathcal{H} \cdot \mathcal{I}(\eta < -1/\log \gamma) \quad (11)$$

where the second mixture component involves a continuous distribution, \mathcal{H} , restricted to the interval $[0, -1/\log \gamma)$, thereby enforcing the aforementioned sufficient condition. In our experience, posterior inferences on η are relatively robust to the continuous prior distribution \mathcal{H} provided the prior is not highly concentrated on a small part of the half-open interval $[0, -1/\log \gamma)$.

When $\eta = 0$, we have a *zero-order Sticky PDP*. On the other hand, when $\eta > 0$, we obtain a *first order Sticky PDP*. In the following situations, some important consequences of specification (10) are:

1. **Zero-order Sticky PDP:** The p customers act identically and independently of each other. That is, when $\eta = 0$, each customer independently chooses restaurant 1 (or 2) with probability equal to the baseline proportion of ρ_1 (or ρ_2).
2. **First order Sticky PDP and ratio e_{j-1}/η large:** Customer j acts approximately independently of the history. Specifically, somewhat similarly to customer 1, customer j chooses restaurant 1 (2) with probability approximately, but not exactly equal to the baseline proportion of ρ_1 (ρ_2). In other words, at large distances, consecutive customers do not appreciably influence each other's choices.
3. **First order Sticky PDP and ratio e_{j-1}/η small:** In the limit as $e_{j-1}/\eta \rightarrow 0$, the restaurant choice of customer j becomes non-random and restaurant g_j has the same label as cuisine s_{j-1} of the previous customer. In other words, at infinitesimal distances, the inter-probe dependencies resemble those of a hidden Markov model.

Posterior inferences on dependence parameter η are therefore of interest. Prior specification (11) allows the data to direct the choice of the model's order through the posterior probability, $P[\eta = 0 \mid \mathbf{X}]$. An empirical average estimate of this probability is readily available from an MCMC sample.

Choice of cuisine s_j and table v_j Within restaurant g_j , customer j selects cuisine-section s_j with distribution \mathcal{Q}_{g_j} , defined earlier in expression (8). For a graphical depiction, see the middle panel of Figure 2, where $g_j = 1$. That is, customer j , having already chosen restaurant 1, must now choose a cuisine section. Restaurant 2 has been greyed out because it is no longer accessible. In the lower panel of Figure 2, we find that the customer finally picked section 1, i.e. $s_j = 1$.

Among the previous $(j - 1)$ customers, consider the subset of customers who had also chosen cuisine-section s_j in restaurant g_j . The number of such customers is denoted by p_{j-1} and is equal to $\sum_{l=1}^{j-1} \mathcal{I}(g_l = g_j, s_l = s_j)$. Let the number of tables occupied by these p_{j-1} customers in that restaurant section be $M_{j-1} \geq 0$. Recall that all customers seated at a table are served the same dish, chosen from the cuisine menu (in this case, cuisine s_j) by the first customer at that table. If $M_{j-1} > 0$, that is, if customer j is not the first patron of the restaurant section, then let $\phi_{g_j s_j k}$ denote the dish from cuisine s_j served to the $p_{j-1,k}$ previous customers already seated at table k , where $k = 1, \dots, M_{j-1}$. Clearly, $p_{j-1,k} = \sum_{l=1}^{j-1} \mathcal{I}(g_l = g_j, s_l = s_j, v_l = k)$. Furthermore, $p_{j-1} = \sum_{k=1}^{M_{j-1}} p_{j-1,k}$. That is, the number of people who had selected section s_j in restaurant g_j before customer j , equals the number of people seated at all the occupied tables in the restaurant section.

Recall that a new customer may sit at an already occupied table or at a new table. Two of these possibilities are illustrated in the lower panel of Figure 2. For a PDP with mass parameter α_{s_j} and discount parameter $d_{s_j} \in [0, 1)$, the predictive distribution of table v_j selected by customer j takes the form:

$$P\left(v_j = k \mid p_{j-1,1}, \dots, p_{j-1,M_{j-1}}\right) \propto \begin{cases} p_{j-1,k} - d_{s_j} & \text{if } k = 1, \dots, M_{j-1}, \\ \alpha_{s_j} + M_{j-1}d_{s_j} & \text{if } k = (M_{j-1} + 1), \end{cases} \quad (12)$$

where the second line corresponds to customer j sitting at a new table, in which case the updated number of occupied tables becomes $M_j = M_{j-1} + 1$. Otherwise, if customer j sits at a previously occupied table, then $M_j = M_{j-1}$. Obviously, $p_j = p_{j-1} + 1$.

Distribution (12) implies that customer j is more likely to choose already occupied tables with greater number of occupants, positively reinforcing the selected table's popularity for future customers. The number of occupied tables stochastically increases with the PDP mass and discount parameters. When discount parameter $d_{s_j} = 0$, we obtain the well-known Pòlya urn scheme for Dirichlet processes (Ferguson 1973b) for section s_j .

In this application, PDPs act as effective dimension reduction devices because the random number of occupied tables is much smaller than the number of customers. Specifically, as the number of patrons in the restaurant section grows, i.e. as $p_j \rightarrow \infty$, the number of occupied tables, M_j , is asymptotically equivalent to

$$\begin{cases} \alpha_{s_j} \log p_j & \text{if } d_{s_j} = 0 \\ T_{d_{s_j}, \alpha_{s_j}} p_j^{d_{s_j}} & \text{if } 0 < d_{s_j} < 1 \end{cases} \quad (13)$$

for a positive random variable $T_{d_{s_j}, \alpha_{s_j}}$. Refer to Lijoi & Prünster (2010) for the general result.

Previous works have exploited PDPs and Dirichlet processes to induce sparsity in unrelated investigations. For example, see Medvedovic et al. (2004), Kim et al. (2006), Dunson et al. (2008), Dunson & Park (2008), and Guha & Baladandayuthapani (2016).

Choice of dish θ_j If customer j sits at a previously occupied table, he or she is served the dish previously selected by the first customer to occupy that table. Otherwise, if a new table is chosen, customer j must pick a dish from menu distribution W_{s_j} . The dish that customer j is served represents the probe-specific random effect θ_j and has the distribution:

$$\theta_j \begin{cases} = \phi_{g_j s_j v_j} & \text{if } v_j = 1, \dots, M_{j-1}, \\ \sim W_{s_j} & \text{if } v_j = (M_{j-1} + 1). \end{cases} \quad (14)$$

If customer j sits at a new table, i.e. if $v_j = (M_{j-1} + 1)$, then the number of occupied tables becomes $M_j = M_{j-1} + 1$, and the newly selected dish $\theta_j = \phi_{g_j s_j M_j} \sim W_{s_j}$ is served to all future customers who choose to sit at table M_j . Otherwise, if customer j sits at an already occupied table, then $M_j = M_{j-1}$ and $\theta_j = \phi_{g_j s_j v_j}$. A consequence of specifications (12) and (14) is that, although each restaurant offers both cuisines and potentially serves every dish, the relative popularity of the dishes are restaurant-specific.

The aforementioned process continues for the subsequent franchise customers $(j + 1), \dots, p$. As seen in expression (10), a factor influencing the restaurant choice of a customer chooses is the cuisine selected by the previous customer. Additionally, expression (8) guarantees that a cuisine is more popular at its namesake restaurant. This results in a customer being more likely to select the same cuisine as the previous customer, and thereby facilitates lengthy runs of differential or non-differential states of the probes. In addition to achieving dimension reduction, the proposed Sticky PDP models serial dependencies in the two-state differential status of adjacent probes as a decreasing function of the inter-probe distances.

2.1.4 Latent clusters and their differential states

The notion of latent clusters, introduced earlier in expression (3), involves allocating all probes with identical random effects to the same cluster. Returning to the MRF metaphor, we observe that a cluster therefore consists of customers having the same dish. Recall that customers seated at a table are served the same dish, although different tables at both the restaurants may serve the same dish. By aggregating MRF customers seated at tables serving identical dishes, irrespective of the restaurant, we can infer in a straightforward manner the probe-cluster allocation variables c_1, \dots, c_p , and therefore, q , the random number of latent clusters. Additionally, by inspecting the

cuisine to which a cluster-specific dish belongs, we are able to infer the common differential state shared by all probes allocated to that cluster. For example, the cluster-specific dishes that belong to cuisine 2 identify the set of differential clusters, \mathcal{D} , defined in equation (4).

From expression (13), we find that the number of occupied tables is usually much smaller than the number of franchise customers, p . Since multiple tables may serve the same dish, the number of latent clusters is usually much smaller than the occupied tables. With high posterior probability, this implies that the unknown number of latent clusters, q , is much smaller than the number of probes, p .

2.1.5 Sticky PDP hyperpriors

Appropriate priors are assumed for mass parameters β , α_1 , and α_2 appearing in expressions (5) and (12). Mean μ_G and variance τ_G^2 of base distribution G_0 in expression (5) are jointly given a normal-inverse gamma prior. Baseline differential proportion, ρ_2 , and speciality-cuisine popularity parameter, γ , are assigned independent uniform(0, 1) priors.

Discount parameter d_2 . Consider the differential state cuisine menu, W_2 , in definition (7). Applying standard asymptotic theory, it can be shown that, when the number of treatments $T \rightarrow \infty$, each atom of W_2 has T univariate elements that are asymptotically i.i.d. G. Furthermore, as T grows, it can be shown that this causes the latent differential probe clusters to be not only identifiable in the limit, but also consistently detected. Refer to Section 4 of Guha & Baladandayuthapani (2016) for a detailed discussion of this remarkable asymptotic phenomenon in standard PDP settings. Parameter d_2 is therefore given the mixture prior:

$$d_2 \sim \frac{1}{2}\delta_0 + \frac{1}{2}U(0, 1)$$

where $d_2 = 0$ corresponds to a Dirichlet process. This provides the necessary flexibility so that the data can choose between a Dirichlet process and a more general PDP for a suitable clustering pattern of the differential probes.

For example, probe allocation patterns that are characteristic of non-Dirichlet PDPs, such as power law decays in the cluster sizes and relatively large numbers of small-sized clusters, would cause parameter d_2 to exclude 0 in the posterior. On the other hand, allocation patterns that are more typical of Dirichlet processes, such as exponentially decaying cluster sizes dominated by a few large clusters, would result in high posterior probabilities being assigned to the point mass at 0. A proof of the intrinsically different allocation patterns of Dirichlet process and PDP priors is given in Theorem 2.1 of Guha & Baladandayuthapani (2016).

Since distribution G is discrete, all atoms of the T -variate distribution W_2 may not be unique. This is indeed not uncommon for $T = 2$ treatments. However, as T grows, and provided the number of probes, p , grows at a slower-than-exponential rate as T , the probability that any two allocated atoms are identical, rapidly decays to 0. The proof is similar to that given in Section 2.3 of Guha & Baladandayuthapani (2016) where the result is derived for a relatively simple zero-order stochastic process in regression problems not related to differential analysis. We have verified this fact in our simulation studies on differential analysis datasets. In several hundred artificial datasets generated from the proposed Sticky PDP, for $p = 1,500$ probes and with T as small as four, no two atoms of distribution W_2 allocated to the p probes were found to be identical.

Discount parameter d_1 . Lastly, consider cuisine menu W_1 is defined in (5). The additional flexibility provided by PDP allocation patterns is not essential for non-differential probes. This is because the allocation patterns of distribution W_1 are driven by the cluster patterns of the univariate quantity, ψ , in (5). As is well documented, the allocation patterns of univariate objects are unidentifiable (e.g., Frühwirth-Schnatter 2006). Consequently, we set PDP discount parameter $d_1 = 0$, reducing the two PDPs associated with the non-differential state (i.e. cuisine 1) to Dirichlet processes.

Figure 3 displays a directed acyclic graph showing the relationships among the BayesDiff model parameters.

2.2 General form of the Sticky PDP

Going beyond differential analysis applications, a Sticky PDP is characterized by the following general properties:

Property 1: Let set \mathcal{G} contain a countable number of generative *groups*. Each group $g \in \mathcal{G}$ contains a countable number of group-specific regular PDPs. The PDPs are identified by a combination of the group label g and an integer-valued *state*, $s \in \mathcal{S} \subset \mathcal{N}$, the set of natural numbers. That is, the regular PDPs comprising a Sticky PDP have bivariate labels, $(g, s) \in \mathcal{G} \times \mathcal{S}$.

Property 2: The regular PDPs may have equal or unequal discount parameters, mass parameters, and/or base distributions. For every $(g, s) \in \mathcal{G} \times \mathcal{S}$, let the corresponding PDP be $\mathcal{W}_{gs}(d_s, \alpha_s, W_s)$.

With \mathcal{P}_{gs} denoting a random realization of the PDP's stick-breaking distribution, we have

$$\begin{aligned}
\mathcal{P}_{gs} &= \sum_{v=1}^{\infty} \pi_{gsv} 1_{\phi_{gsv}} \quad \text{where the } T\text{-variate atoms} \\
\phi_{gsv} &\stackrel{iid}{\sim} W_s, \quad \text{for index } v \in \mathcal{N}, \text{ and probabilities} \\
\pi_{gs1} &= V_{gs1}, \quad \pi_{gsh} = V_{gsh} \prod_{v=1}^{h-1} (1 - V_{gsv}), \quad h > 1, \quad \text{with} \\
V_{gsh} &\stackrel{indep}{\sim} \text{beta}(1 - d_s, \alpha_s + h d_s).
\end{aligned} \tag{15}$$

Notice that base distribution W_s in \mathcal{R}^T is determined by the state s but not group g . On the other hand, the atoms and their associated probabilities in distribution \mathcal{P}_{gs} may depend on both group and state.

If set \mathcal{S} contains multiple states, assume that the set of base distributions $\{W_s : s \in \mathcal{S}\}$ is such that two PDPs associated with unequal states will almost surely have non-intersecting sets of atoms. That is, whenever $s_1^* \neq s_2^*$, the intersection of the random sets of the atoms $\{\phi_{g_1^* s_1^* v}\}_{v=1}^{\infty}$ and $\{\phi_{g_2^* s_2^* v}\}_{v=1}^{\infty}$ of stick-breaking distributions $\mathcal{P}_{g_1^* s_1^*}$ and $\mathcal{P}_{g_2^* s_2^*}$ is almost surely empty.

Property 3: For probe $j = 1, \dots, p$, the label of the PDP generating random effect θ_j is denoted by $(g_j, s_j) \in \mathcal{G} \times \mathcal{S}$, and $\theta_j \mid \mathcal{P}_{g_j s_j} \stackrel{indep}{\sim} \mathcal{P}_{g_j s_j}$. Equivalently, random effect θ_j equals atom $\phi_{g_j s_j v_j}$ with probability $\pi_{g_j s_j v_j}$ for index $v_j \in \mathcal{N}$.

Property 4: Given group g_j for the j^{th} probe, the state of the PDP generating random effect θ_j is randomly selected as follows:

$$s_j \mid g_j \sim \mathcal{Q}_{g_j}$$

where for every $g \in \mathcal{G}$, \mathcal{Q}_g denotes a group-specific probability mass function on the set \mathcal{S} ; thus, $\sum_{s \in \mathcal{S}} \mathcal{Q}_g(s) = 1$.

Property 5: (*Markov property*) For probe $j > 1$, given the variables associated with the preceding probes, group variable g_j has a mass function depending on random vector θ_{j-1} and inter-probe distance e_{j-1} :

$$g_j \sim \mathcal{F}_{\theta_{j-1}, e_{j-1}}$$

where, for every $\theta \in \mathcal{R}^T$ and $e > 0$, $\mathcal{F}_{\theta, e}$ denotes a probability mass function on the set \mathcal{G} , so that $\sum_{g \in \mathcal{G}} \mathcal{F}_{\theta, e}(g) = 1$. For the first probe, group g_1 follows a categorical distribution, \mathcal{F}_0 , on the set \mathcal{G} .

Model	\mathcal{G}	$\mathcal{W}_{gs}(d_s, \alpha_s, W_s)$	\mathcal{P}_{gs}	$\mathcal{F}_{\theta, e}$
HDP-HMM	\mathcal{N}	$\mathcal{W}_g(0, \alpha, W)$, countably infinite W	$\sum_{v=1}^{\infty} \pi_{gv} 1_{\phi_v}$	Point mass at $\sum_{v=1}^{\infty} v \cdot \mathcal{I}(\theta = \phi_v)$
Finite HMM	$\{1, \dots, K\}$	$\mathcal{W}_g(0, \alpha, W)$, discrete W with $K < \infty$ atoms	$\sum_{v=1}^K \pi_{gv} 1_{\phi_v}$	Point mass at $\sum_{v=1}^K v \cdot \mathcal{I}(\theta = \phi_v)$
HDP	$\{1, \dots, K\}$	$\mathcal{W}_g(0, \alpha, W)$, countably infinite W	$\sum_{v=1}^{\infty} \pi_{gv} 1_{\phi_v}$	$1_{\{g\}}$, prespecified $g \in \mathcal{G}$
PDP	$\{1\}$	$\mathcal{W}(d, \alpha, W)$	$\sum_{v=1}^{\infty} \pi_v 1_{\phi_v}$	$1_{\{1\}}$
Dirichlet process	$\{1\}$	$\mathcal{W}(0, \alpha, W)$	$\sum_{v=1}^{\infty} \pi_v 1_{\phi_v}$	$1_{\{1\}}$
Finite mixture	$\{1\}$	$\mathcal{W}(0, \alpha, W)$, discrete W with $K < \infty$ atoms	$\sum_{v=1}^K \pi_v 1_{\phi_v}$	$1_{\{1\}}$

Table 1: Examples of Sticky PDPs. Set \mathcal{N} represents the natural numbers. All the above examples correspond to singleton set $\mathcal{S} = \{1\}$ and degenerate distribution $\mathcal{Q}_g = 1_{\{1\}}$. Refer to the description in Section 2.2 for the notation.

In addition to extending PDPs to discrete time series type data, the general formulation of Sticky PDPs offers a diverse palette of parametric and nonparametric models for capturing the distinctive features of the data in different applications. The range of models includes Dirichlet processes, PDPs, infinite HMMs, hierarchical Dirichlet process (HDP) (Müller et al. 2004, Teh et al. 2006), finite HMMs, nested Chinese restaurant processes (Blei & Jordan 2005), nested Dirichlet processes (Rodriguez et al. 2008), and analysis of densities models (Tomlinson & Escobar 2003). Some examples are presented in Table 1; as suggested by the form of distribution $\mathcal{F}_{\theta, e}$ in the table, the first two models are first order Sticky PDPs. The Sticky PDP of Section 2.1 is a special case with two groups and two states.

We observe that the first order models displayed in Table 1 are multiple-group, *single-state* models, and that their dependencies are the same irrespective of the inter-probe distances. In contrast, as noted in Consequences 2 and 3 of Section 2.1.3, the proposed Sticky PDP for differential analysis behaves similarly to two-state hidden Markov models for very small inter-probe distances, and similarly to finite mixture models for relatively large distances. For differential analysis, this offers a key advantage in datasets with widely varying inter-probe distances, as discussed in detail in Section 1. The differential and non-differential probes are allowed to have different cluster allocation patterns depending on the differential status of the adjacent probes. These are some of the features that make Sticky PDPs ideally suited for differential analysis, and are primarily facilitated by the two-group, two-state construct.

3 Posterior Inferences for Differential Analysis

Due to the analytical intractability of the BayesDiff model, we rely on MCMC methods for posterior inferences and detection of the differential probes.

3.1 MCMC Strategy

The model parameters are initialized using naïve estimation techniques and iteratively updated by MCMC techniques until the chain converges to the posterior. We split the MCMC updates into three blocks. An outline of the MCMC procedure is as follows:

1. **Restaurant-cuisine-table-dish choice $(g_j, s_j, v_j, \boldsymbol{\theta}_j)$ of customer j :** For each probe $j = 1, \dots, p$, we sample the 4-tuple $(g_j, s_j, v_j, \boldsymbol{\theta}_j)$ given the 4-tuples of the other $(p - 1)$ probes. This is achieved by proposing a new value of $(g_j, s_j, v_j, \boldsymbol{\theta}_j)$ from a carefully constructed approximation to its full conditional, and by accepting or rejecting the proposed 4-tuple of probe-specific parameters in a Metropolis-Hastings step. The procedure is repeated for all p probes to complete the block of MCMC updates.

We give here an intuitive description of the details. Further calculations are available in Supplemental Materials. For the j th probe, $1 < j < p$, the choice of restaurant g_j depends on the triplets of the two immediately adjacent probes. Specifically, as discussed in Section 2.1.3, and as graphically shown in the upper and middle panel of Figure 2, the restaurant selected by a customer depends on the cuisine of the previous customer. Then, within restaurant g_j , the customer chooses cuisine s_j with a restaurant-specific probability. Finally, the customer may either sit an existing table, in which case they must eat the same dish as everyone already sitting at that table, or the customer may open a new table and order a dish from cuisine menu s_j . The generation strategy for table and dish depends on the cuisine, as discussed below.

Cuisine $s_j = 1$ Evaluating the posterior probability of table v_j involves integrating the Gaussian likelihood of column vector $\mathbf{z}_j = (z_{1j}, \dots, z_{nj})'$ with respect to the cuisine 1 menu, i.e. $\boldsymbol{\theta}_j \sim W_1$. Recall that the cuisine 1 menu has the special structure (5), allowing its reduction to a univariate quantity distributed as G . This random distribution itself follows a Dirichlet process conditional prior with a base distribution that is a mixture of known atoms (given the 4-tuples of the other probes) and Gaussian distribution G_0 . This conjugate hierarchical structure allows the calculation of table and dish choice for cuisine 1 in computationally closed form.

Cuisine $s_j = 2$ This situation is more complicated because the Gaussian likelihood must be integrated with respect to prior distribution W_2 of the cuisine 2 dishes. Unlike cuisine 1, this is not possible in computationally closed form because menu structure (7) cannot be reduced to a univariate quantity. In other words, for cuisine 2 (i.e. the differential state), the Dirichlet process conditional prior for distribution G is non-conjugate.

We utilize an auxiliary variable approach. Given the current set and frequency of atoms of distribution G in the other $(p - 1)$ probes, we first compute a finite mixture approximation, G^* , to the Dirichlet process conditional prior for G , as in Ishwaran & Zarepour (2002). Then, using prior (7), it is possible to approximate the posterior probability of customer j joining an existing table or sitting at a new table, irrespective of the dishes. This allows us to generate the table selection, v_j . Finally, we propose the dish, $\theta_j = \phi_{g_j s_j v_j}$. If table v_j is one of the already existing tables, then the customer simply chooses the common, table-specific dish. Otherwise, we sequentially generate from the posterior the T elements representing the new dish. This is done using the corresponding treatment-specific elements of vector $\mathbf{z}_j = (z_{1j}, \dots, z_{nj})'$ and finite mixture G^* , with the restriction that not all T atoms of vector θ_j are equal. The Metropolis-Hasting step compensates for any approximations and produces post-burn-in samples from the BayesDiff model posterior.

Latent clusters As discussed in Section 2.1.4, the probe-cluster allocations c_1, \dots, c_p are immediately available from the restaurant-cuisine-table allocations (g_j, s_j, v_j) of the p probes. The q latent clusters, along with their allocated probes, and the set of differential clusters \mathcal{D} , are also immediately available.

2. **Latent vectors** $\lambda_1, \dots, \lambda_q$: Since each latent vector is of length T , there are Tq latent vector elements, not all of which are necessarily distinct because of the Dirichlet process prior on distribution G . Although the latent vector elements are available from Block 1, mixing of the MCMC chain is considerably improved by an additional block of updates of the latent vector elements conditional on the p probe-cluster allocations. As the following calculation shows, this can be done by Gibbs sampling.

Since a non-differential cluster's latent vector consists of a single value repeated T times, the number of *distinct* latent vector elements is no more than $(q_1 + Tq_2)$. Given the current probe-cluster allocations, suppose there are m_k probes associated with latent cluster k , where $k = 1, \dots, q$. Let $q_2 = |\mathcal{D}|$ be the number of differential clusters, so that $q_1 = q - q_2$ is the number of non-differential clusters.

Non-differential clusters For these clusters, the latent vector $\boldsymbol{\lambda}_k$ takes the form, $\boldsymbol{\lambda}_k = \psi_k \mathbf{1}_T$ for some $\psi_k \in \mathcal{R}$. Given the other $(q - 1)$ latent vectors, assumptions (5) and (7) imply that parameter ψ_k has a Dirichlet process conditional prior. The base distribution of the Dirichlet process is a mixture of a continuous distribution, $G_0 = N(\mu_G, \tau_G^2)$, and the univariate atoms located at the “known” elements of the other $(q - 1)$ latent vectors. The sufficient statistic for ψ_k is

$$\begin{aligned} \bar{y}_k &= \frac{1}{nm_k} \sum_{j=1}^p \sum_{i=1}^n (z_{ij} - \xi_i - \chi_j) \mathcal{I}(c_j = k) \\ &\sim N\left(\psi_k, \frac{\sigma^2}{nm_k}\right) \quad \text{for cluster } k \notin \mathcal{D}. \end{aligned}$$

Since the Dirichlet process conditional prior is conjugate to this normal likelihood, parameter ψ_k could be updated by Gibbs sampling (Escobar 1994, MacEachern 1994, Escobar & West 1995).

Differential clusters For these clusters, some of the T elements of latent vector $\boldsymbol{\lambda}_k = (\lambda_{1k}, \dots, \lambda_{Tk})'$ could be tied, but at least two elements must be unequal. Denote these restrictions on $\boldsymbol{\lambda}_k$ by \mathcal{A} . For a treatment t , let the remaining $(T - 1)$ elements of vector $\boldsymbol{\lambda}_k$ be denoted by $\boldsymbol{\lambda}_{-tk}$.

Imagine updating element λ_{tk} assuming that $\boldsymbol{\lambda}_{-tk}$ and the remaining $(q - 1)$ latent vectors are known. Vector $\boldsymbol{\lambda}_{-tk}$ and restriction \mathcal{A} imply a possibly restricted support, \mathcal{A}_t , for parameter λ_{tk} . Observe that the support is unrestricted, i.e. $\mathcal{A}_t = \mathcal{R}$, if at least two elements of $\boldsymbol{\lambda}_{-tk}$ differ. Similarly to non-differential clusters, it can be shown that element λ_{tk} follows a Dirichlet process conditional prior restricted to the support \mathcal{A}_t , and that the base distribution is a mixture of a normal distribution and univariate atoms. The sufficient statistic for latent vector element λ_{tk} is

$$\begin{aligned} \bar{y}_{tk} &= \frac{1}{n_t m_k} \sum_{j=1}^p \sum_{i:t_i=t} (z_{ij} - \xi_i - \chi_j) \mathcal{I}(c_j = k) \\ &\sim N\left(\lambda_{tk}, \frac{\sigma^2}{n_t m_k}\right) \quad \text{for treatment } t = 1, \dots, T, \text{ and cluster } k \in \mathcal{D}, \end{aligned}$$

where n_t is the number of individuals associated with treatment t . The conjugate structure implies that parameter λ_{tk} could be generated from its full conditional by a rejection sampler on set \mathcal{A}_t coupled with standard Gibbs proposals for conjugate Dirichlet processes. In practice, the acceptance rates of the rejection sampler are very high for T as small as 3 or 4, and are nearly 100% for larger T . This is because the posterior probability of support set \mathcal{A}_t tends

to 1 as T grows. An intuitive explanation for this asymptotic property is provided in Section 2.1.5 following the prior specification of discount parameter d_2 .

Scalability Due to the intensive nature of the aforementioned one-parameter-at-a-time Gibbs sampling updates, the Metropolis-Hastings algorithm of Guha (2010) can be applied to significantly speed up the updates. Briefly, the algorithm proceeds by detecting “neighborhoods” of latent vector elements that are approximately i.i.d. in posterior, and that have not yet been updated in the current MCMC cycle. Despite the nomenclature, these neighborhoods are not necessarily spatially proximal. The updated values for an entire neighborhood of elements are then proposed as i.i.d. draws from the approximate, common full conditional. Any approximation in the proposals is corrected by a MetropolisHastings step to obtain post-burn-in MCMC samples from the true posterior. This procedure is repeated until all Tq latent vector elements have been updated. Relatively to standard Gibbs samplers, ten- to hundred-fold speedups are obtained by this fast MCMC strategy. A similar strategy could be applied in Block 1 to obtain order of magnitude speedups for the restaurant-cuisine-table-dish parameters of the p customers.

3. **Remaining model parameters:** These parameters include the subject-specific random effects ξ_1, \dots, ξ_n , probe-specific random effects χ_1, \dots, χ_p , range parameter η , differential PDP discount parameter d_2 , univariate Dirichlet process mass parameter β , Dirichlet process base distribution parameters μ_G and τ_G^2 , and variance parameter σ^2 . All of these parameters can be updated by standard MCMC techniques.

3.2 Detection of Differential Probes with FDR Control

As an optional inferential step, a Bayesian approach for controlling the false discovery rate (FDR) (Newton et al. 2004) could be applied for more accurately detecting the differential probes, i.e. the probes j with differential state, $s_j = 2$.

Specifically, let q_0 be the nominal FDR level and let ω_j be the posterior probability of probe j being differential, so that $\omega_j = P[s_j = 2 \mid \mathbf{X}]$. An empirical average estimate, $\hat{\omega}_j$, is available from the MCMC sample. To achieve the desired FDR level in calling the differential probes, we first rank all the probes in decreasing order of $\hat{\omega}_j$. Let $\hat{\omega}_{(1)} > \hat{\omega}_{(2)} > \dots > \hat{\omega}_{(p)}$ denote the ordered posterior probability estimates. For each $b = 1, \dots, p$, we calculate the posterior expected FDR resulting from calling the first b probes in decreasing order of $\hat{\omega}_j$, as follows:

$$\widehat{\text{FDR}}_b = \frac{\sum_{j=1}^p (1 - \hat{\omega}_j) \mathcal{I}(\hat{\omega}_j \geq \hat{\omega}_{(b)})}{\sum_{j=1}^p \mathcal{I}(\hat{\omega}_j \geq \hat{\omega}_{(b)})} = \frac{\sum_{j=1}^b (1 - \hat{\omega}_{(j)})}{b} \quad (16)$$

where the simplified expression follows from the fact that the $\hat{\omega}_j$'s are sorted. Finally, we pick the largest value of b , denoted by b^* , for which $\widehat{\text{FDR}}_b < q_0$. The detection rule that labels as differential the first b^* probes arranged in decreasing order of $\hat{\omega}_j$, achieves the nominal FDR level of q_0 .

4 Simulation Studies

To evaluate the ability of the BayesDiff procedure in learning the dependence structure of DNA methylation data, we analyzed artificial datasets with $T = 5$ treatments. The accuracy of BayesDiff in detecting the differentially methylated probes was compared with established differential methylation procedures and general statistical techniques for multigroup comparison.

Generation strategy Proportions representing DNA methylation data were generated using the logit transformation in equation (1). The distances between the p probes were actual sequences of $(p-1)$ inter-probe distances from the motivating TCGA dataset, scaled to add to 1. In order to capture the complexity of methylation data, such as the existence of multiple latent methylation states (e.g. CpG islands and shores), different read depths across CpGs and the incomplete conversion of bisulphite sequencing, the generation strategy was partly based on techniques implemented in WGBSSuite, a flexible stochastic simulation tool for generating single-base resolution methylation data (Rackham et al. 2015). However, the generation procedure differed from WGBSSuite in some respects. Specifically, it accommodated more than two treatments ($T > 2$) and incorporated serial dependence not only in the methylation states, but also in the differential states of the probes.

The probes-specific read depths were generated as $n_j \stackrel{iid}{\sim} \text{Poisson}(50)$. No subject-specific random effects were included in the generation strategy. The true probe-specific random effects $\chi_1^{(0)}, \dots, \chi_p^{(0)}$ were generated as follows:

1. The true methylation status of the probes, denoted by $h_1^{(0)}, \dots, h_p^{(0)}$, using the 4-state *distance-based* HMM of Rackham et al. (2015), with the states respectively representing the methylated, first transit, demethylated, and second transit states.
2. Set the baseline methylation levels for the methylated, (first or second) transit, and demethylated states as $p_{\text{methylated}} = 0.8$, $p_{\text{transit}} = 0.5$, and $p_{\text{un-methylated}} = 0.2$, respectively.

α_1	α_2	d_2	β	γ	ρ_2	μ_G	τ_G^2	τ_χ^2
20	20	0.33	20	0.9	0.1	0	1	0.1225

Table 2: True parameter values used to generate the artificial datasets.

3. For $j = 1, \dots, p$, define the mean probe-specific random effect as follows:

$$\tilde{\chi}_j^{(0)} = \begin{cases} \log\left(\frac{p_{\text{methylated}}}{1-p_{\text{methylated}}}\right) & \text{if } h_j = 1 \text{ (i.e. methylated state),} \\ \log\left(\frac{p_{\text{transit}}}{1-p_{\text{transit}}}\right) & \text{if } h_j = 2, 4 \text{ (first or second transit state),} \\ \log\left(\frac{p_{\text{demethylated}}}{1-p_{\text{demethylated}}}\right) & \text{if } h_j = 3 \text{ (i.e. demethylated state).} \end{cases}$$

4. Independently generate the true probe-specific random effects: $\chi_j^{(0)} \sim N(\tilde{\chi}_j^{(0)}, \tau_\chi^2)$ for probe $j = 1, \dots, p$.

Noise and dependence levels We investigated four scenarios corresponding to the combinations of two noise levels and two dependence levels. For each scenario, 20 datasets were independently generated, with each dataset consisting of $p = 500$ probes and $T = 5$ treatments with 4 samples each, i.e. a total to $n = 20$ samples. The low noise level corresponded to true variance parameter, $\sigma_0^2 = 0.36$; equivalently, to a signal-to-noise of $R_0^2 \approx 70\%$. The high noise level corresponded to $\sigma_0^2 = 1$ or $R_0^2 \approx 40\%$. The true between-probe dependencies comprised of two levels: no serial correlation (i.e. a zero-order Sticky PDP) with $\eta_0 = 0$, and positive serial correlation (i.e. a first order Sticky PDP) with $\eta_0 = 0.004$. Although $\eta_0 = 0.004$ may appear to be small, its value is calibrated to the inter-probe distances. Specifically, when the distance between two adjacent probes is equal to the standardized average distance of $\bar{e} = 1/(p-1) = 1/499$, $\eta_0 = 0.004$ gives an affiliation of $r_0 = 0.6$ in equation (9). Since affiliations are bounded above by 1, $\eta_0 = 0.004$ represents fairly high inter-probe dependence. For convenience, we will refer to the two dependence levels as “no-correlation” and “high correlation.” The other model parameters were common for the four scenarios and are displayed in Table 2. Setting a true baseline differential proportion of $\rho_2 = 0.1$ resulted in approximately 10% true differentially methylated CpGs in each dataset.

Posterior inferences Assuming all model parameters to be unknown, each artificial dataset was analyzed using the BayesDiff procedure. The true generation mechanism differed in key respects from the BayesDiff model subsequently used to analyze the data. For example, unlike the 4-state HMM of the generation strategy, the probe-specific random effects χ_j were analyzed using a BayesDiff model that ignored the first order dependence, and instead, relied on a 3-state finite mixture model representing the methylated, transit, and unmethylated states. Additionally, in contrast to

the missing subject-specific random effects during data generation, the BayesDiff procedure assumed that the random effects were i.i.d. normal with zero mean.

To assess the accuracy of BayesDiff in detecting the absence or presence of inter-probe serial correlation, in the no-correlation ($\eta_0 = 0$) situation, we evaluated $\log \left(\frac{P[\eta=0|\mathbf{X}]}{P[\eta>0|\mathbf{X}]} \right)$, the log-Bayes factor comparing zero order to first order Sticky PDPs. In the high correlation ($\eta_0 = 0.04$) situation, we evaluated $\log \left(\frac{P[\eta>0|\mathbf{X}]}{P[\eta=0|\mathbf{X}]} \right)$, the log-Bayes factor comparing first order to zero order Sticky PDPs. Thus, in a given scenario, a large positive value of the corresponding log-Bayes factor would constitute strong evidence that BayesDiff detects the correct model order.

Although conceptually straightforward, the estimation of Bayes factors requires multiple MCMC runs, even for relatively simple parametric models (Chib 1995). Basu & Chib (2003) extended the estimation strategy to infinite dimensional models such as Dirichlet processes. However, the computational costs are prohibitive for big datasets and multiple MCMC runs for estimating Bayes factors would stretch available computational resources far beyond their present-day limits. Faced with these challenges, we have relied on an alternative strategy for estimating the upper bounds of log-Bayes factors using a single MCMC run. As it turns out, this is often sufficient to infer the Sticky PDP model orders. Let Θ^- denote all BayesDiff model parameters except η . In the high correlation situation, applying Jensen’s inequality, a lower bound for the corresponding log-Bayes factor is found to be $E \left[\log \left(\frac{P[\eta>0|\mathbf{X}, \Theta^-]}{P[\eta=0|\mathbf{X}, \Theta^-]} \right) \mid \mathbf{X} \right]$. Unlike log-Bayes factors, this lower bound can be easily estimated by an empirical average estimate based on a single MCMC run. In the no-correlation situation, a lower bound for the log-Bayes factor, $\log \left(\frac{P[\eta=0|\mathbf{X}]}{P[\eta>0|\mathbf{X}]} \right)$, can be similarly derived.

For each of the four generation scenarios, box plots of these estimated lower bounds for the 20 datasets are depicted in Figure 4. Except for the high noise–no-correlation scenario, for which the results were inconclusive, the estimated lower bounds of the log-Bayes factors in favor of the true correlation structure were all positive and sufficiently large. In the low noise–no-correlation scenario, BayesDiff decisively favored zero-order models, and the smallest lower bound among the 20 datasets was 13.9, corresponding to Bayes factors exceeding $e^{13.9} = 1,088,161$. The 25th percentile of these lower bounds was 30.9, corresponding to Bayes factors exceeding $e^{30.9} = 2.63 \times 10^{13}$. This is strong evidence that the BayesDiff approach is reliable in this scenario. For the high-correlation scenarios, the estimated lower bounds were even higher, showing that BayesDiff overwhelmingly favors first order models when the data are, in fact, serially correlated.

Comparisons with other methods We evaluated the success of the BayesDiff procedure in detecting disease genomic signatures and made comparisons with six well-known procedures. These included general statistical techniques for multigroup comparisons, namely, one-way analysis of variance (ANOVA) and the Kruskal-Wallis test. We also made comparisons with some methods

specially developed for detecting differential methylation in more than two treatments: COHCAP (Warden et al. 2013), methylKit (Akalin et al. 2012), BiSeq (Hebestreit et al. 2013), and RADMeth (Dolzhenko & Smith 2014).

The ANOVA and the Kruskal-Wallis test procedures were applied separately on each probe after applying the inverse-logit transform. Being specifically designed for differential methylation analysis, the COHCAP method was directly applied to the generated proportions of the synthetic data. The remaining three methylation-related methods are designed for bisulfite sequencing, which consists of the total methylation reads for each measured CpG site. For these methods, the methylation reads for each probe was obtained by multiplying the proportion methylation values by the total read. The bandwidth smoothing parameter of the method BiSeq was tuned to optimize the overall detection. For all six methods, the probe-specific p-values were obtained. The probes whose test p-values were less than the desired significance level were labeled as differential for that method.

We computed the receiver operating characteristic (ROC) curves for differential probe detection for all seven methods. The ROC curves, averaged over the 20 datasets under each simulation scenario, are shown in Figure 5. The ROC curves for the individual datasets are available in Supplementary Materials. In all except the high-noise-no-correlation scenario, BayesDiff uniformly outperformed the other methods, as indicated by the fact that the areas under the ROC curves were greater for BayesDiff. Even in the high-noise-no-correlation scenario, we find that BayesDiff performed better in the low FPR region. As expected, all seven methods had lower accuracies for the higher noise levels. The performance of BayesDiff was significantly better than the competing methods in the high correlation scenarios, suggesting that the incorporation of between-probe dependencies greatly improved its accuracy.

For a quantitative assessment, we calculated the area under curve (AUC) for the ROC curves, declaring the method as the most reliable when it has the largest AUC in a given scenario. In addition, since researchers typically focus on small false positive rates (FPRs), that is, small significance levels, we also calculated the measures, AUC_{20} and AUC_{10} . AUC_{20} (AUC_{10}) is defined as the area under the ROC curve multiplied by 5 (10) when the FPR does not exceed 0.2 (0.1). The multiplicative factor ensures that the areas potentially vary between 0 and 1. The three versions of AUC are presented in Table 3.

We find that in three of the four scenarios, BayesDiff had the largest overall AUC, and furthermore, had vastly improved reliability for low FPRs. For example, consider the low noise-high correlation scenario. The overall AUC for BayesDiff was 0.031 greater than that for ANOVA. In contrast, the gains for BayesDiff, relative to ANOVA, were +0.098 for AUC_{20} and +0.136 for AUC_{10} . The advantages of BayesDiff were even greater relative to the other competing methods. In the high

noise–low-correlation scenario, BayesDiff had a relatively low AUC, as mentioned earlier. However, even in this scenario, it had the greatest AUC_{20} and AUC_{10} values among all the methods. Additionally, for a nominal FDR level of $q_0 = 0.05$, the achieved FDR of BayesDiff was between 0 and 0.03 in every dataset and simulation scenario. These results demonstrate the ability of BayesDiff to accurately detect the differential probes even in challenging situations where the FPR is small.

5 Data Analysis

We returned to the motivating DNA methylation dataset consisting of the four types of GI cancer: stomach adenocarcinoma (STAD), liver hepatocellular carcinoma (LIHC), esophageal carcinoma (ESCA) and pancreatic adenocarcinoma (PAAD). Applying the BayesDiff procedure, we detected the differentially methylated CpG loci among the cancer types.

Data processing The dataset was obtained from The Cancer Genome Atlas project, which is publicly available through The Genomic Data Commons (GDC) Data Portal (Grossman et al. 2016). The data are available from the Illumina Human Methylation 450 platform for each of 485,577 probes at the CpG sites. At the time of analysis, the dataset consisted of 1,224 tumor samples.

The analysis was performed on a gene-by-gene basis. We picked a set of 443 genes involving mutation in at least 5% of the samples. To ensure that all CpG sites potentially related to a gene were included in the analysis, we selected all sites located within 50K base pairs outside the gene body, specifically, upstream from the 5' end and downstream from the 3' end. The number of gene-specific CpG sites ranged from 1 to 769, and are displayed in Figure 6(a). As a final preprocessing step, we eliminated the 25 genes mapped to 20 CpG sites or less. This is primarily because many existing statistical methods are effective in genes for which the number of CpG sites, p , is small, and also because the methylation patterns of short genes are usually of lesser interest in cancer investigations.

Inference procedure The data were analyzed using the proposed BayesDiff approach. Since DNA methylation data consist of proportions, the logit transformation was applied in expression (1). The subject-specific random effects were assumed to be distributed as $\xi_i \stackrel{iid}{\sim} N(0, \tau_\epsilon^2)$. The MCMC procedure of Section 3.1 was applied to obtain posterior samples for each gene. For detecting differentially methylated CpG sites, we applied the Bayesian FDR control procedure of Section 3.2 with a nominal FDR of $q_0 = 0.05$.

Results For each gene, Figure 6(b) displays 95% credible intervals for lower bounds of log-Bayes factors of a first versus zero-order model, i.e., $\eta = 0$ versus $\eta > 0$ in expression (9) for the inter-probe affiliations. Models with first order dependence are overwhelmingly favored for a majority of the genes, suggesting that statistical techniques that do not account for dependence between neighboring CpG sites would be less effective for these data.

Among the differentially methylated CpG sites detected by our approach, approximately 40.6% of the sites were located outside the gene bodies. Figure 7 displays the associations between detected methylation status and positions of the CpG sites. For our analysis, we have defined “near the 5’ (3’) end” as the CpG sites located within one-fourth length of the gene body, either inside or outside the gene boundary, and closer to the transcription start (termination) site. Our results indicate that the proportion of differential methylation is higher for CpG sites inside the gene body, and that most differentially methylated loci are situated within the gene body, as is well known from numerous previous studies. However, our analysis also revealed significant amounts of differential methylation outside the gene body. Despite the common belief that DNA methylation analysis should focus on the 5’ end region, we have found that CpG sites near the 3’ ends also display considerable degrees of differential methylation. These findings support the recommendations of Irizarry et al. (2009) that the investigation of DNA methylation alteration should be conducted on a higher resolution, epigenome-wide basis.

Among the differentially methylated sites detected by BayesDiff, we estimated the pairwise differences between the random effects associated with the four cancer types. Site-wise summaries of the largest pairwise differences of the cancer-specific effects are plotted in Figure 8. None of the four cancer types displayed consistent hypermethylation or hypomethylation across all the genes or entire chromosomes. However, we found that LIHC is frequently differentially methylated relative to one of the other cancer types, implying that it is the most volatile disease with respect to DNA methylation.

Figure 9 displays the detailed differential methylation pattern for the top two mutated genes, TP53 and TTN. An obvious feature of both the genes is that the detected differential methylation of the CpG sites is highly serially correlated. For gene TP53, there are almost no differentially methylated loci within the gene body. The 3’ end region outside the gene body has a cluster of differentially methylated loci, for which cancer type STAD is mostly hypermethylated. The results for gene TTN tell a quite different story: most of the differentially methylated loci are inside the gene body and near the 5’ end. Cancer type LIHC is hypomethylated compared to PAAD around the 5’ end region, but it is hypermethylated compared to STAD near the 3’ end. Finally, genes with at least 90% differentially methylated sites are listed in Table 4, along with the largest pairwise

difference between the four cancer types among the differentially methylated loci. The number of CpG sites within each segment is listed in Supplementary Materials.

Existing medical literature both supports and complements our findings. For example, hypermethylation of the EDNRB and SLIT2 genes have been found in STAD (Tao et al. 2012, Kim et al. 2016). Gene FBN2 was hypermethylated in ESCA (Tsunoda et al. 2009). While several studies have found that the gene and protein expressions of ABC transporter genes, such as ABCC9, are useful for understanding the prognosis of esophageal cancer (Vrana et al. 2018), we conclude that hypermethylation of ABCC9 is a major difference between cancer types ESCA and LIHC. Gene FLRT2 is a potential tumor suppressor that is hypermethylated and downregulated in breast cancer (Bae et al. 2017). Our results indicate that this gene is also hypermethylated in cancer type STAD versus LIHC. Mutations in SPTA1 gene has been linked with PAAD (Murphy et al. 2013). The BayesDiff results indicate that hypermethylation of this gene distinguishes PAAD from LIHC.

Accounting for data characteristics In genomic studies, a statistical model should be able to account for the probe-specific means and variances. This is especially important in multiple-testing based approaches where the first two sample moments must be plausibly explained by the fitted model to avoid making misleading biological interpretations (Subramaniam & Hsiao 2012). From this perspective, certain aspects of the BayesDiff model, such as a platform-specific transformation and a common variance σ^2 a priori unrelated to the mean of the Gaussian likelihood (1), may appear to be restrictive. However, even though the BayesDiff model was not specifically constructed to match data summaries such as sample moments, in practice, the nonparametric nature of the Sticky PDP allows the model posterior to flexibly adapt to the features of the data such as sample moments, thereby properly accounting for the mean-variance relationships in a robust manner.

For example, consider the top 2 mutated genes, TP53 and TTN, discussed in Figure 9. The ability of the BayesDiff model to account for the sample moments of the gene-specific probes can be demonstrated as follows. Given the inter-probe distances, the joint posterior of the BayesDiff parameters induces predictive distributions on the n measurements for each probe. Functionals of these predictive distributions, such as the probe-specific sample moments, can be quickly estimated by post-processing the MCMC sample. For the two genes, Figure 10 reveals that the predicted sample moments under BayesDiff closely match the actual first and second sample moments, with correlations exceeding 99% in each plot. Similar results were observed in other datasets that we have analyzed.

Posterior consistency results in the nonparametric Bayesian literature typically assume i.i.d. observations from processes convolved with Gaussian noise (e.g. Ghosal et al. 1999). Because of this, it is difficult to give a general theoretical explanation for this interesting phenomenon. Theoretical

results are even more limited for proportion, nominal or ordinal measurements, and for first order stochastic processes. However, intuitive explanations are possible in some situations. For example, consider an investigation in which the column vectors $\mathbf{x}_1, \dots, \mathbf{x}_p$ are a priori exchangeable and, additionally, the row vectors of data matrix \mathbf{X} are also a priori exchangeable. These assumptions are valid when there is little or no serial dependence among the p probes and the n subjects are randomly sampled from a large population. In particular, exchangeability does not preclude situations where the patient-specific and/or probe-specific summaries of matrix \mathbf{X} can be classified into ‘high’ and ‘low’ level categories. After applying a bijective transformation, e.g. $z(x) = \log(1 + x)$ in the case of RNASeq count data, it is appropriate to fit a zero-order BayesDiff model to these data.

Now, by De Finetti’s theorem, the exchangeable column vectors $\mathbf{x}_1, \dots, \mathbf{x}_p$ of length n are i.i.d. realizations of an underlying true process, \mathcal{X} , in \mathcal{R}^n . The transformed column vectors, $\mathbf{z}_1, \dots, \mathbf{z}_p$, are then i.i.d. realizations of an equivalent process, $\mathcal{Z} = \tilde{z}(\mathcal{X})$, where \tilde{z} denotes univariate transformation z applied elementwise to a vector of length n . After accounting for the subject-specific and probe-specific main effects, the Sticky PDP of Section 2.1 essentially approximates process \mathcal{Z} by a mixture of Gaussian densities with an adaptive number of components. It is common knowledge among practitioners that, when p is large, Gaussian mixtures with enough components and a shared variance σ^2 are often very successful in approximating a wide variety of continuous processes. Consequently, functionals of \mathcal{Z} , such as sample moments of i.i.d. vectors from $\mathcal{X} = \tilde{z}^{-1}(\mathcal{Z})$, can also be accurately estimated by the posterior distributions of Sticky PDPs.

6 Discussion

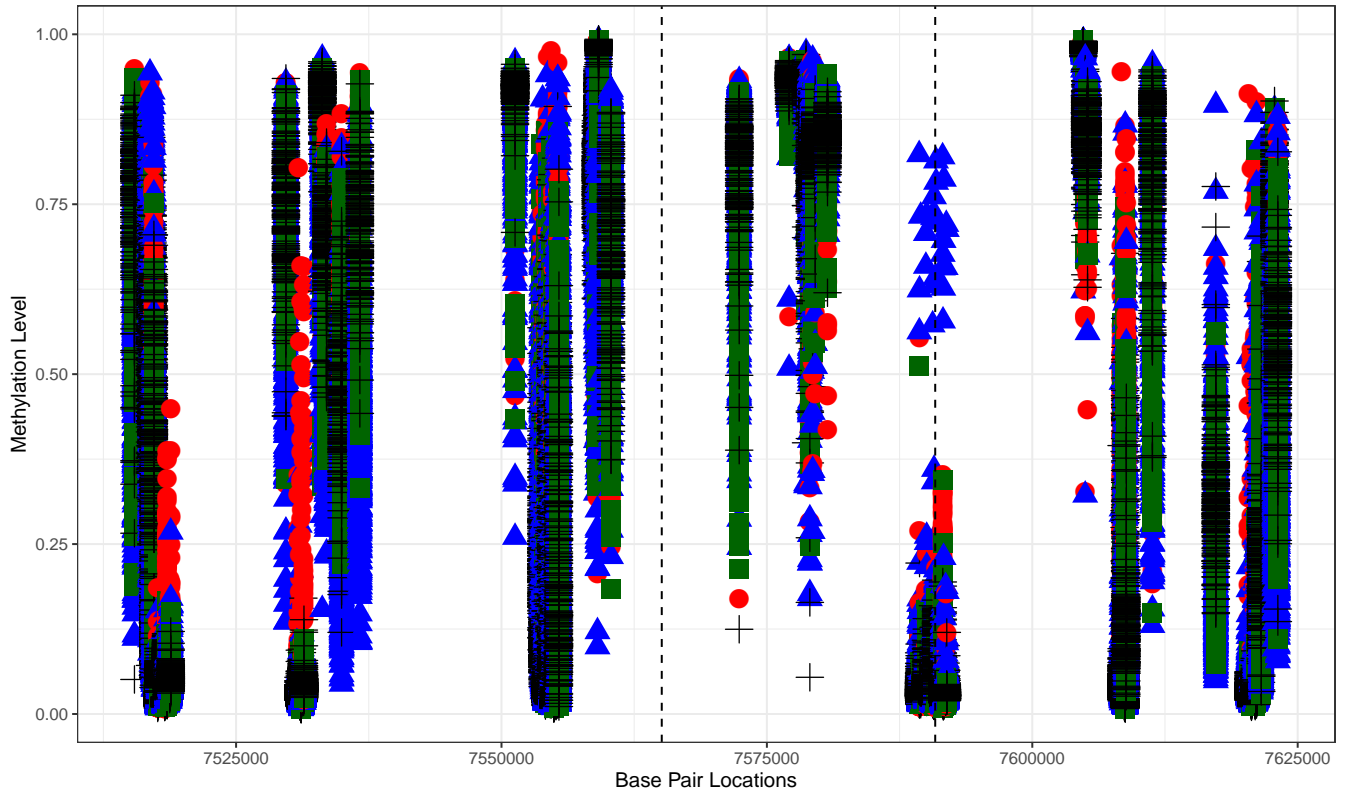
DNA methylation data in GI cancer, like many other kinds of omics data, exhibit complex structures due to unknown biological mechanisms and distance-dependent serial correlations among neighboring probes. The identification of differential signatures among different groups of samples is crucial for developing targeted treatments for disease. This paper formulates a flexible approach called BayesDiff that is applicable to omics datasets of different sizes and scales and to multiple treatments. The technique relies on a novel Bayesian mixture model called the Sticky PDP or the multicuisine restaurant franchise. In addition to allowing simultaneous inferences on the probes, the model accommodates distance-based serial dependence and accounts for the complex interaction patterns prevalent in cancer data. The Sticky PDP encompasses several well-known Bayesian mixture models as special cases.

A computationally efficient MCMC strategy for detecting the differential probes is developed. The success of the BayesDiff procedure in differential DNA methylation, relative to well-established

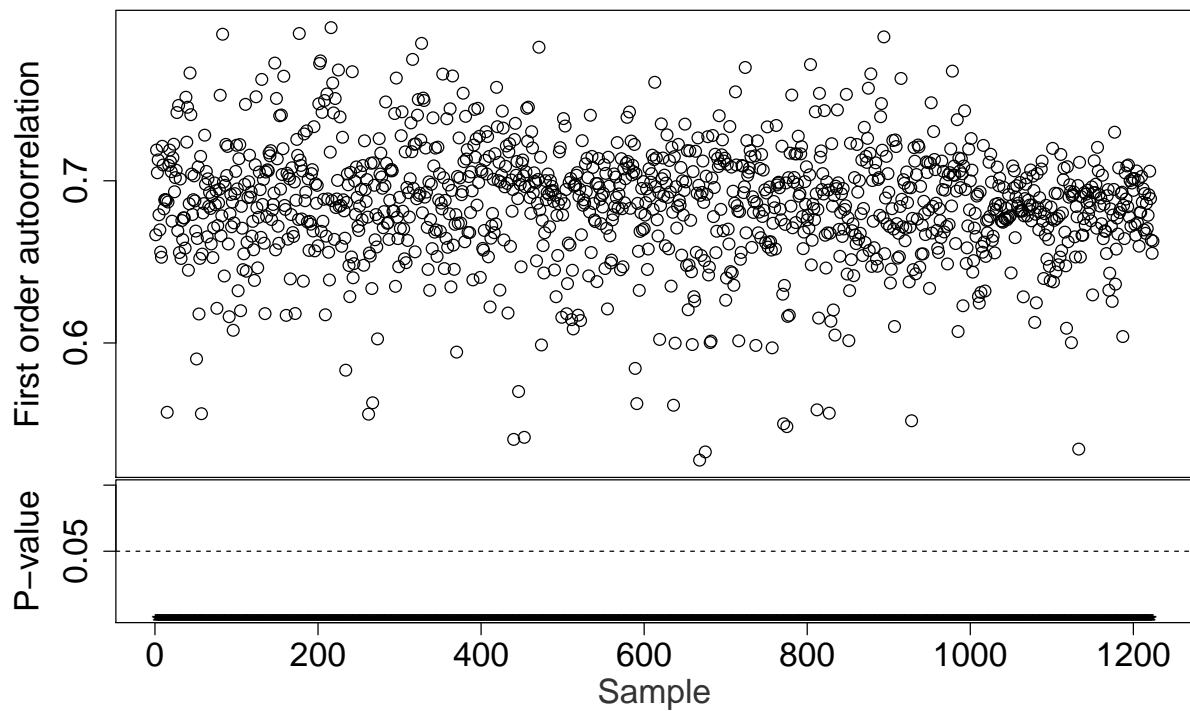
methodologies, is exhibited via simulation studies. The new technique is applied to the motivating TCGA dataset to detect the differential genomic signature of four types of upper GI cancer. The results both support and complement various known facts about the epigenomic differences between these cancer types, while also revealing a set of genes exhibiting high proportions of differentially methylated CpG sites. These results emphasize the need for further investigation to better understand the molecular characterizations of upper GI cancer.

In addition to providing a good fit for the data, a statistical model must be able to account for features of the dataset such as sample moments. The success of the BayesDiff model in this regard is demonstrated in Section 5 for the upper GI dataset. It must be emphasized, however, that there may be other datasets where BayesDiff is less successful in accounting for the data characteristics. This could be due to many reasons, e.g. as the number of probes grows, there is slow asymptotic convergence of the posterior to the true generative process, and so, p is insufficiently large to provide a good match for the data. In such situations, more flexible global transformations (Li et al. 2016) or variance-stabilizing transformations (Durbin et al. 2002) could be used. Alternatively, we could replace the global transformations of the measurements, $z_{ij} = z(x_{ij})$, by local Laplace approximations of exponential family likelihoods through link functions, e.g. binomial likelihoods with logit link for proportions, and Poisson or negative binomial likelihoods with log link for count data (Zeger & Karim 1991, Chib & Winkelmann 2001). These approximations rely on the model parameters to produce approximately normal working values with means $\xi_i + \chi_j + \theta_{t_{ij}}$ and variances σ_{ij}^2 that differ across subjects and probes, unlike equation (1), which assumes a shared σ^2 parameter. In this manner, we could extend the BayesDiff procedure to further improve the model fit and better explain the unique characteristics of these datasets.

Ongoing work involves extending the correlation structure to model more sophisticated forms of inter-probe dependence. We are currently developing an R package implementing BayesDiff in a parallel computing framework using graphical processing units. The software will be made available for detecting differential genomic signatures in wide variety of applications. Initial results indicate that dramatic speedups of several orders of magnitude would allow the analysis of user-specified datasets on ordinary personal computers.



(a) Methylation levels of CpG sites near gene TP53.



(b) Estimated first order autocorrelations and hypothesis test p-values for the 1,224 upper GI cancer samples

Figure 1: Exploratory analysis of DNA methylation profiles of upper GI cancer samples available from TCGA. See the text for further explanation.

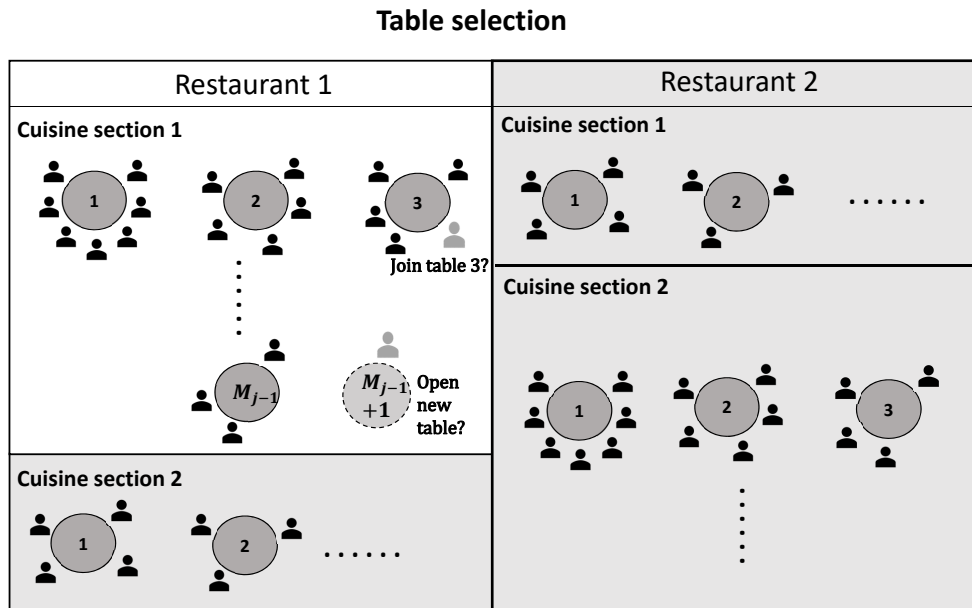
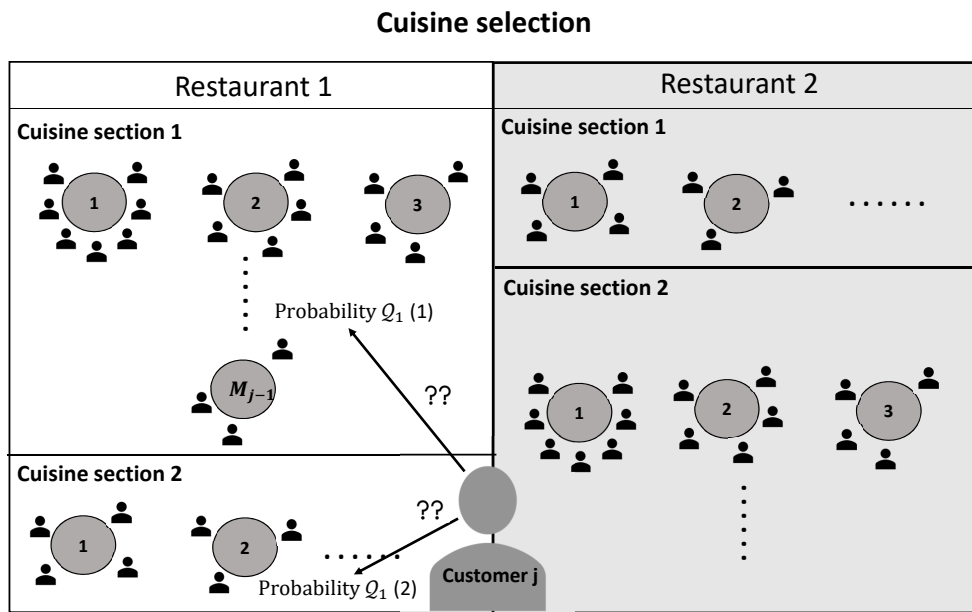
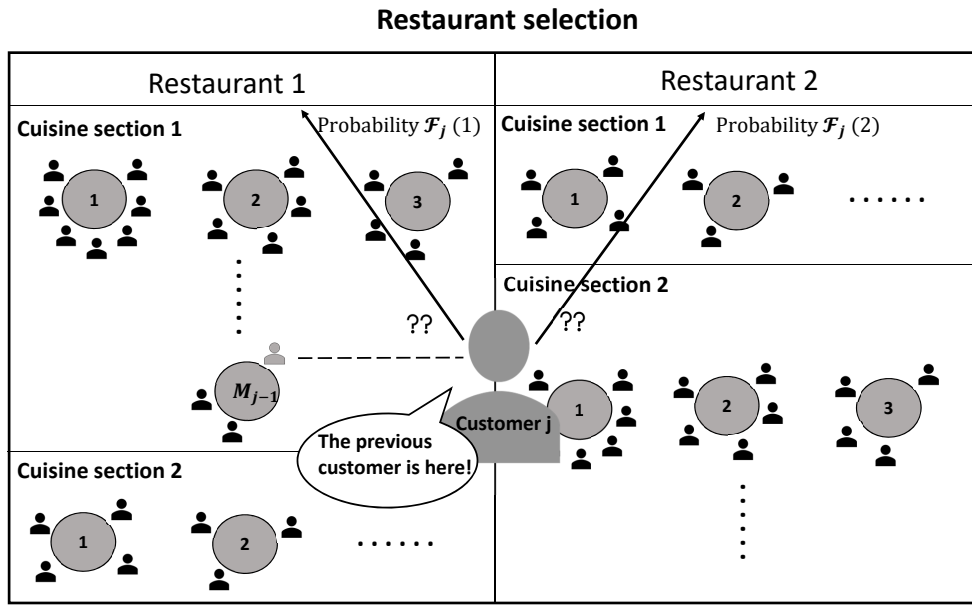


Figure 2: Cartoon representation of the multicuisine restaurant franchise for differential analysis, showing the progressive choice of restaurant, cuisine section, and table by customer j , where $j > 1$. The numbered circles represent the table numbers. See the text in Section 2.1 for further explanation.

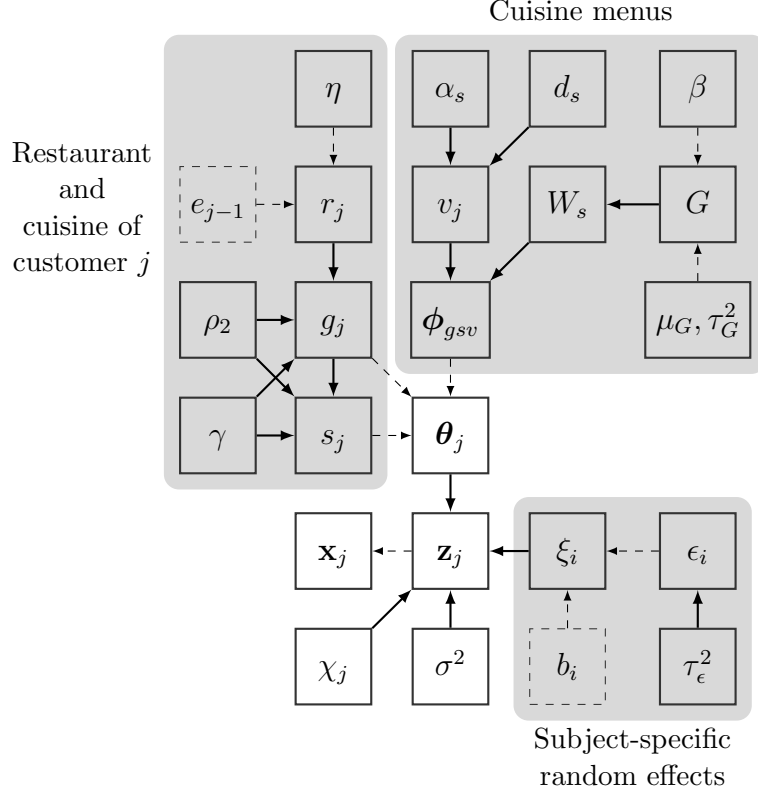


Figure 3: Directed acyclic graph of the BayesDiff model showing the relationships between the model parameters. Solid rectangles represent the data and model parameters. Dashed rectangles represent predetermined constants. Solid arrows represent stochastic relationships, and dashed arrows represent deterministic relationships.

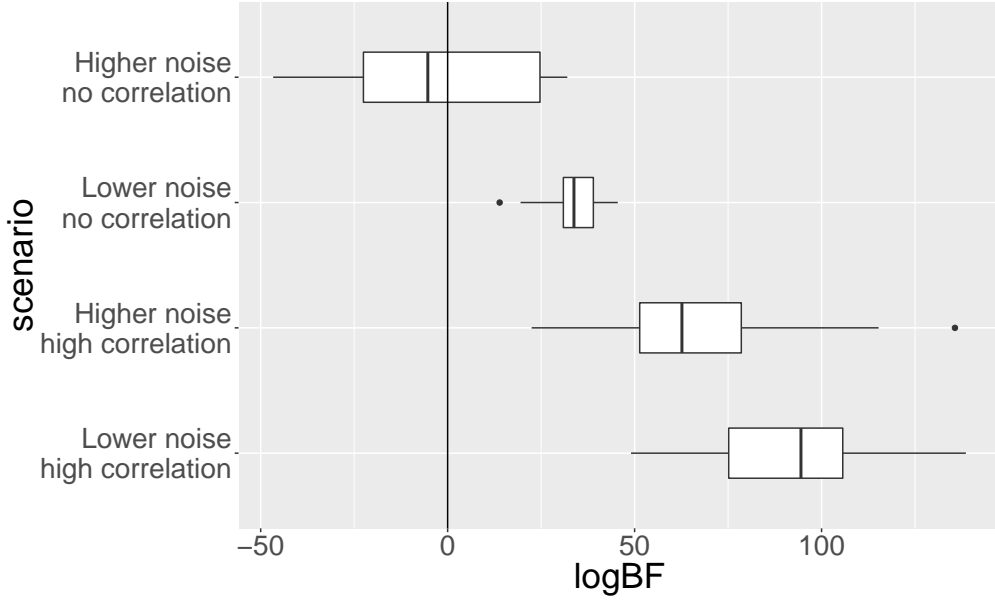
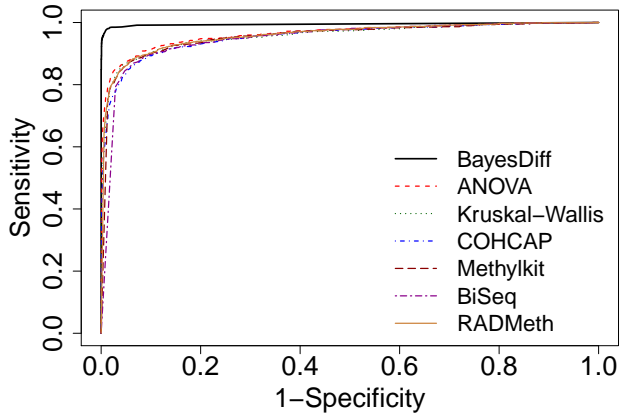
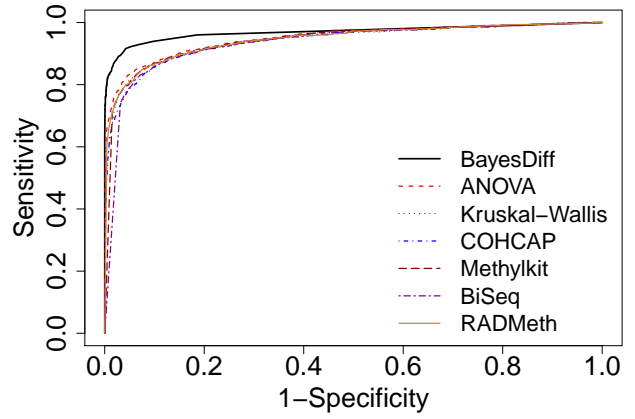


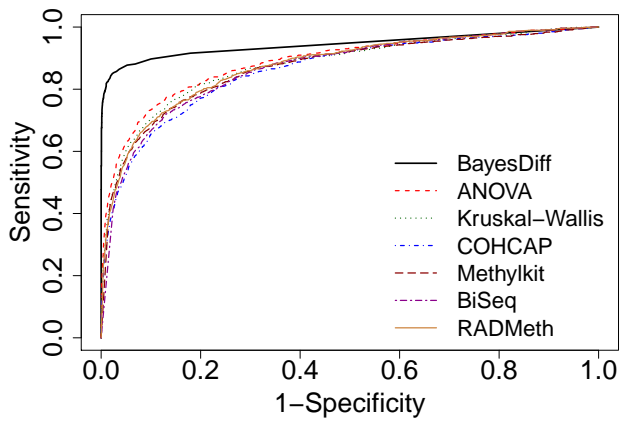
Figure 4: In the simulation study, box plots for the estimated lower bounds of log-Bayes factors in favor of the true model order.



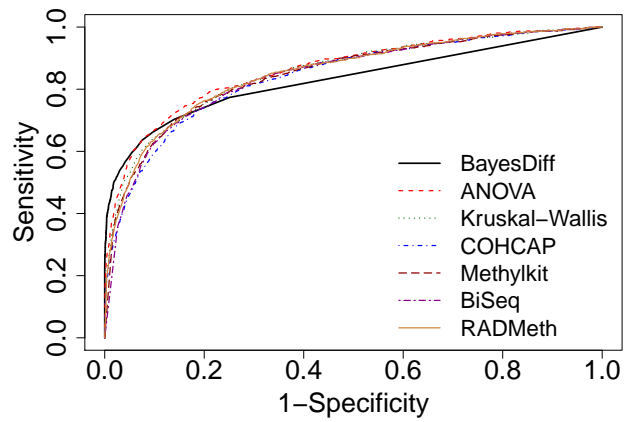
(a) Low noise, high correlation



(b) Low noise, no correlation

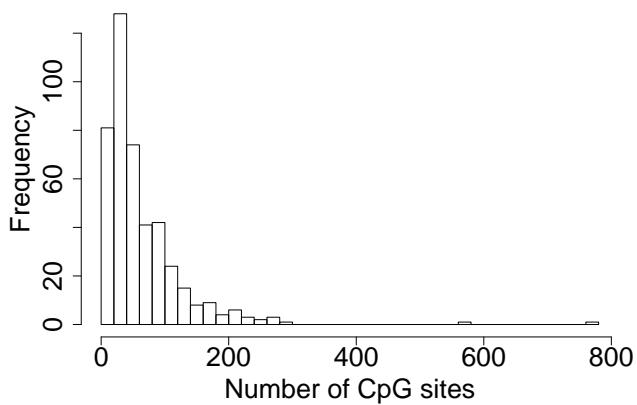


(c) High noise, high correlation

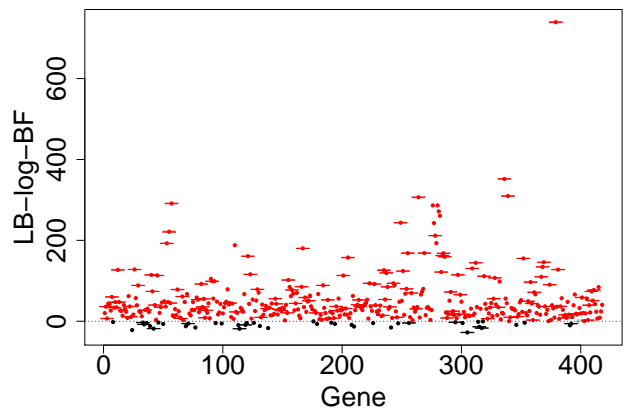


(d) High noise, no correlation

Figure 5: ROC curves, averaged over 20 simulated datasets, for the seven methods and the four simulation scenarios.



(a) Histogram of the number of gene-specific CpG sites

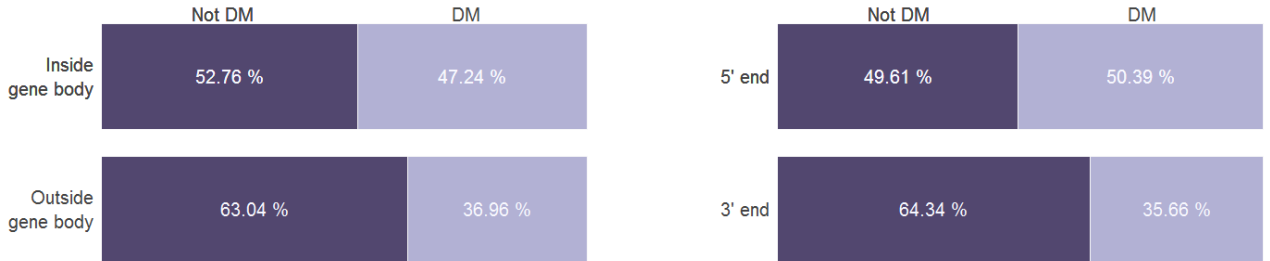


(b) 95% credible intervals for lower bounds of log-Bayes factors of first order versus zero-order models. The intervals whose lower limits are positive are marked in red.

Figure 6: Data analysis plots. See the Section 5 text for further explanation.

		Low noise		High noise	
		High correlation	No correlation	High correlation	No correlation
AUC	BayesDiff	0.995	0.970	0.944	0.830
	ANOVA	0.964	0.949	0.888	0.864
	Kruskal-Wallis	0.958	0.944	0.878	0.854
	COHCAP	0.955	0.941	0.861	0.841
	Methylkit	0.955	0.942	0.869	0.848
	BiSeq	0.949	0.933	0.867	0.845
	RADMeth	0.959	0.944	0.876	0.852
AUC ₂₀	BayesDiff	0.988	0.926	0.884	0.636
	ANOVA	0.891	0.851	0.684	0.628
	Kruskal-Wallis	0.876	0.833	0.657	0.597
	COHCAP	0.856	0.820	0.602	0.556
	Methylkit	0.858	0.819	0.633	0.579
	BiSeq	0.822	0.781	0.607	0.559
	RADMeth	0.871	0.833	0.639	0.588
AUC ₁₀	BayesDiff	0.985	0.901	0.857	0.565
	ANOVA	0.849	0.804	0.586	0.529
	Kruskal-Wallis	0.827	0.773	0.551	0.493
	COHCAP	0.797	0.751	0.492	0.433
	Methylkit	0.794	0.744	0.523	0.458
	BiSeq	0.726	0.673	0.482	0.424
	RADMeth	0.817	0.775	0.531	0.471

Table 3: Areas under ROC curves for the different methods (rows) under the four simulation scenarios (columns). See the text for further discussion.



(a) Contingency table of detected methylation status and location of CpG site with respect to gene body (b) Contingency table of detected methylation status and proximity of CpG site to chromosomal end

Figure 7: Associations of detected methylation status and position of CpG sites.

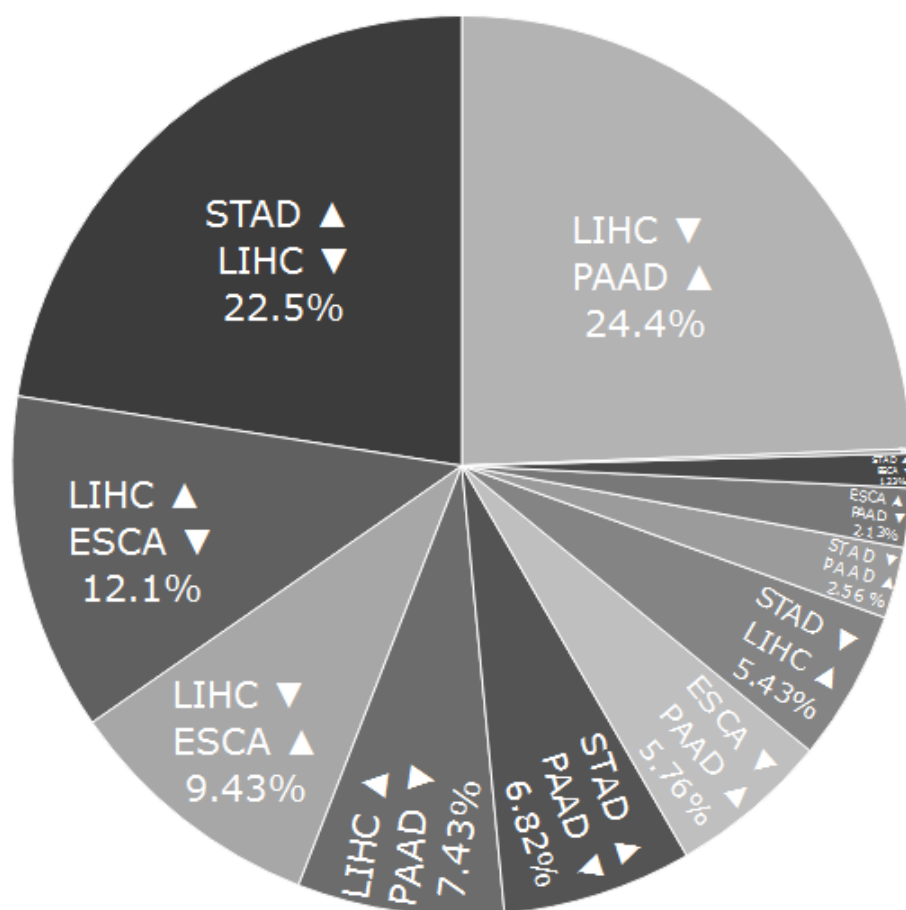


Figure 8: Site-wise summary of the largest pairwise differences of differentially methylated loci among the four upper GI cancer types.

Gene	DM Proportion	Largest Difference	Gene	DM Proportion	Largest Difference
EDNRB	1.00	STAD↑ LIHC↓	SLITRK1	0.96	STAD↑ LIHC↓
PCLO	1.00	PAAD↑ LIHC↓	FLRT2	0.96	STAD↑ LIHC↓
PREX2	1.00	STAD↑ LIHC↓	KCNA1	0.96	STAD↑ LIHC↓
SLIT2	1.00	STAD↑ LIHC↓	TRPA1	0.96	STAD↑ LIHC↓
SLITRK2	1.00	STAD↑ LIHC↓	ADCY8	0.96	STAD↑ LIHC↓
SORCS3	1.00	STAD↑ LIHC↓	CTNNA2	0.95	PAAD↑ LIHC↓
SPHKAP	1.00	ESCA↑ LIHC↓	GRIA2	0.95	STAD↑ LIHC↓
SPTA1	1.00	PAAD↑ LIHC↓	ADGRL3	0.94	PAAD↑ LIHC↓
UNC13C	1.00	PAAD↑ LIHC↓	LRRC7	0.94	STAD↑ LIHC↓
XIRP2	1.00	PAAD↑ LIHC↓	ERBB4	0.93	PAAD↑ LIHC↓
ZNF804B	1.00	STAD↑ LIHC↓	PCDH10	0.93	STAD↑ LIHC↓
TSHZ3	0.97	STAD↑ LIHC↓	SOX11	0.93	STAD↑ LIHC↓
MYO3A	0.97	STAD↑ LIHC↓	NLGN4X	0.93	PAAD↑ LIHC↓
ABCC9	0.97	ESCA↑ LIHC↓	NBEA	0.93	PAAD↑ LIHC↓
EPB41L3	0.97	STAD↑ LIHC↓	CNTN1	0.92	STAD↑ LIHC↓
FBN2	0.97	STAD↑ LIHC↓	GRM5	0.92	PAAD↑ LIHC↓
PCDH17	0.96	STAD↑ LIHC↓	PTPRZ1	0.91	STAD↑ PAAD↓
CDH8	0.96	STAD↑ LIHC↓	EPHA5	0.91	STAD↑ LIHC↓

Table 4: Genes with the overall proportion of differentially methylated CpG sites exceeding 0.9, listed in descending order. The “Largest Difference” column displays which pair-wise difference between the four cancer types is the largest, with the symbol “↑ (↓)” indicating higher (lower) methylation level for one cancer type relative to the other.

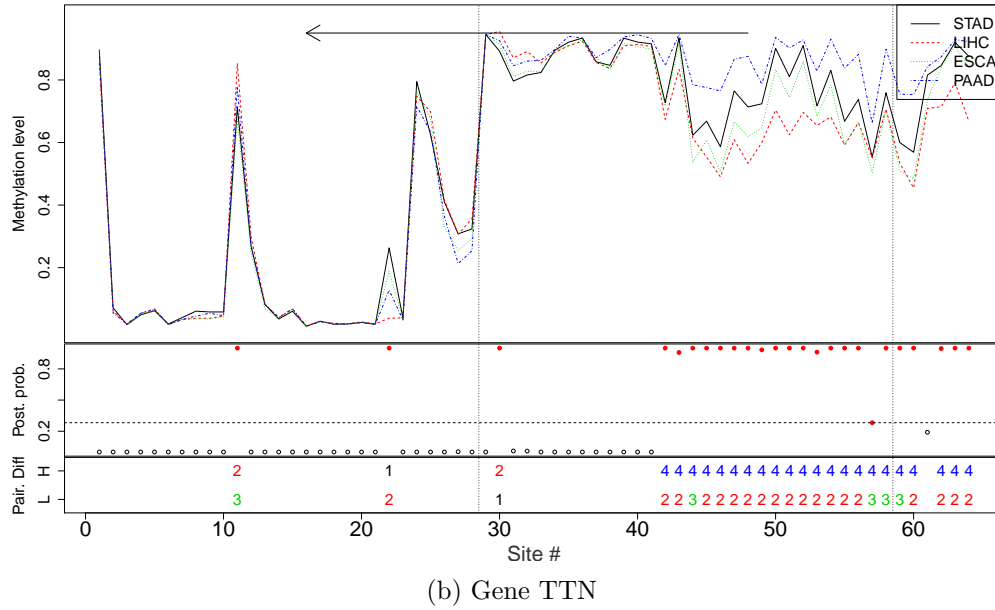
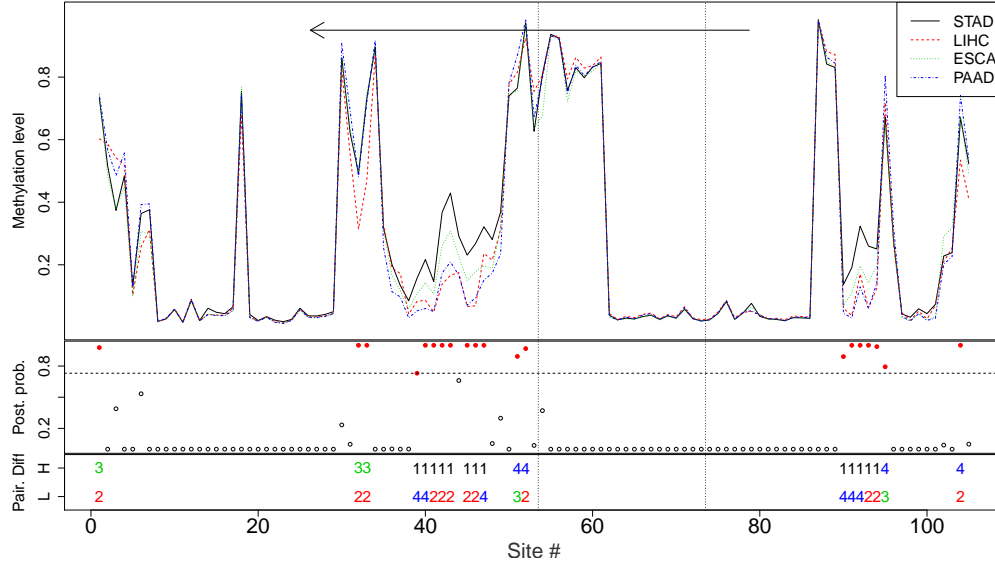
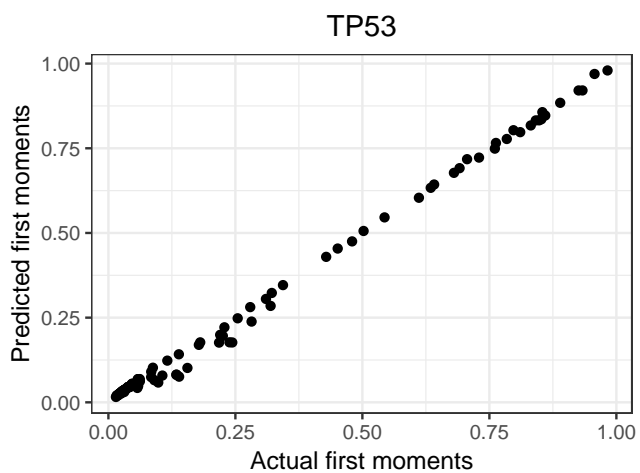
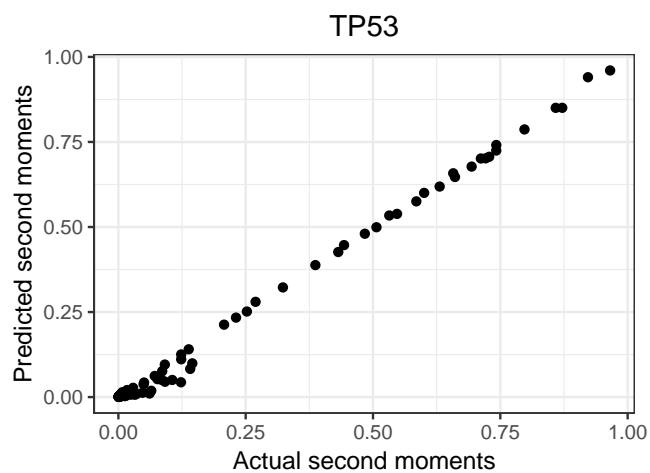


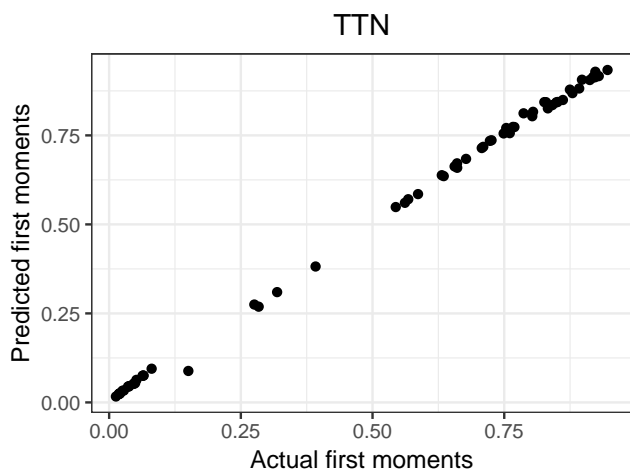
Figure 9: Detailed differential methylation results for the top 2 mutated genes. For each gene, the upper panel shows the mean methylation levels. The middle panel shows the posterior probabilities of each CpG site being differentially methylated, with solid points representing differential methylation and dashed line denoting the corresponding cutoff value. The lower panel indicates the largest pairwise difference between the 4 cancer types. Symbols 1–4 in the lower panel represent GI cancer types STAD, LIHC, ESCA and PAAD, respectively. The vertical dotted lines represent the gene boundaries. The arrow at the top indicates the transcription direction.



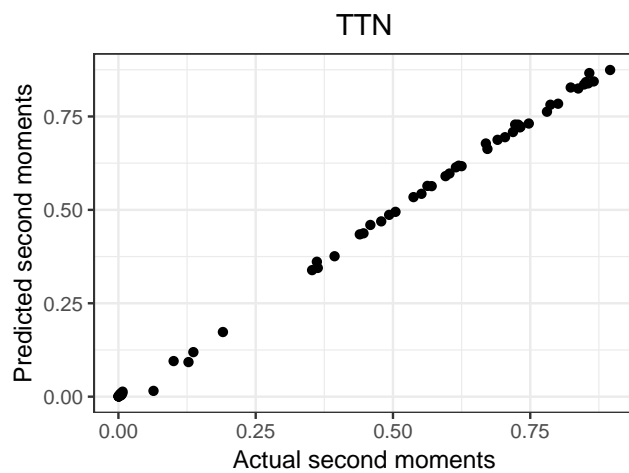
(a) First moments for gene TP53



(b) Second moments for gene TP53



(c) First moments for gene TTN



(d) Second moments for gene TTN

Figure 10: Comparison of predicted and actual sample moments for the 2 top mutated genes

References

- Akalin, A., Kormaksson, M., Li, S., Garrett-Bakelman, F. E., Figueroa, M. E., Melnick, A. & Mason, C. E. (2012), ‘methylkit: a comprehensive r package for the analysis of genome-wide dna methylation profiles’, *Genome biology* **13**(10), R87.
- Bae, H., Kim, B., Lee, H., Lee, S., Kang, H.-S. & Kim, S. J. (2017), ‘Epigenetically regulated fibronectin leucine rich transmembrane protein 2 (flrt2) shows tumor suppressor activity in breast cancer cells’, *Scientific Reports* **7**(1), 272.
- Basu, S. & Chib, S. (2003), ‘Marginal likelihood and bayes factors for dirichlet process mixture models’, *Journal of the American Statistical Association* **98**(461), 224–235.
- Blei, D. M. & Jordan, M. I. (2005), ‘Variational inference for dirichlet process mixtures’, *Bayesian Analysis* **1**, 1–23.
- Chib, S. (1995), ‘Marginal likelihood from the gibbs output’, *Journal of the American Statistical Association* **90**(432), 1313–1321.
- Chib, S. & Winkelmann, R. (2001), ‘Markov chain monte carlo analysis of correlated count data’, *Journal of Business & Economic Statistics* **19**(4), 428–435.
- Dolzhenko, E. & Smith, A. D. (2014), ‘Using beta-binomial regression for high-precision differential methylation analysis in multifactor whole-genome bisulfite sequencing experiments’, *BMC bioinformatics* **15**(1), 215.
- Dunson, D. B., Herring, A. H. & Engel, S. M. (2008), ‘Bayesian selection and clustering of polymorphisms in functionally-related genes’, *Journal of the American Statistical Association* **103**, 534–546.
- Dunson, D. B. & Park, J.-H. (2008), ‘Kernel stick-breaking processes’, *Biometrika* **95**, 307–323.
- Durbin, B., Hardin, J., Hawkins, D. & Roake, D. (2002), ‘A variance-stabilizing transformation for gene-expression microarray data’, *Bioinformatics* **18**, S105–S110.
- Eads, C. A., Lord, R. V., Kurumboor, S. K., Wickramasinghe, K., Skinner, M. L., Long, T. I., Peters, J. H., DeMeester, T. R., Danenberg, K. D., Danenberg, P. V. et al. (2000), ‘Fields of aberrant cpg island hypermethylation in barretts esophagus and associated adenocarcinoma’, *Cancer research* **60**(18), 5021–5026.
- Eckhardt, F., Lewin, J., Cortese, R., Rakyan, V. K., Attwood, J., Burger, M., Burton, J., Cox, T. V., Davies, R., Down, T. A. et al. (2006), ‘Dna methylation profiling of human chromosomes 6, 20 and 22’, *Nature genetics* **38**(12), 1378.
- Escobar, M. D. (1994), ‘Estimating normal means with a dirichlet process prior’, *Journal of the American Statistical Association* **89**(425), 268–277.
- Escobar, M. D. & West, M. (1995), ‘Bayesian density estimation and inference using mixtures’, *Journal of the american statistical association* **90**(430), 577–588.
- Feinberg, A. P. & Tycko, B. (2004), ‘The history of cancer epigenetics’, *Nature reviews. Cancer* **4**(2), 143.

- Feng, H., Conneely, K. N. & Wu, H. (2014), ‘A bayesian hierarchical model to detect differentially methylated loci from single nucleotide resolution sequencing data’, *Nucleic acids research* **42**(8), e69–e69.
- Ferguson, T. S. (1973a), ‘A bayesian analysis of some nonparametric problems’, *The annals of statistics* pp. 209–230.
- Ferguson, T. S. (1973b), ‘A bayesian analysis of some nonparametric problems’, *Annals of Statistics* **1**, 209–223.
- Fox, E., Sudderth, E., Jordan, M. & Willsky, A. (2011), ‘The sticky hdp-hmm: Bayesian nonparametric hidden markov models with persistent states’, *Annals of Applied Statistics* **5**, 1020–1056.
- Frühwirth-Schnatter, S. (2006), *Finite Mixture and Markov Switching Models*, New York: Springer.
- Ghosal, S., Ghosh, J. K. & Ramamoorthi, R. V. (1999), ‘Posterior consistency of dirichlet mixtures in density estimation’, *The Annals of Statistics* **27**, 143–158.
- Gnedin, A. & Pitman, J. (2005), ‘Regenerative composition structures’, *Annals of Probability* **33**, 445–479.
- Graham, D. Y. (2015), ‘Helicobacter pylori update: gastric cancer, reliable therapy, and possible benefits’, *Gastroenterology* **148**(4), 719–731.
- Grossman, R. L., Heath, A. P., Ferretti, V., Varmus, H. E., Lowy, D. R., Kibbe, W. A. & Staudt, L. M. (2016), ‘Toward a shared vision for cancer genomic data’, *New England Journal of Medicine* **375**(12), 1109–1112.
- Guha, S. (2010), ‘Posterior simulation in countable mixture models for large datasets’, *Journal of the American Statistical Association* **105**(490), 775–786.
- Guha, S. & Baladandayuthapani, V. (2016), ‘A nonparametric bayesian technique for high-dimensional regression’, *Electronic Journal of Statistics* **10**, 3374–3424.
- Hamid, J. S., Hu, P., Roslin, N. M., Ling, V., Greenwood, C. M. T. & Beyene, J. (2009), ‘Data integration in genetics and genomics: methods and challenges’, *Human Genomics and Proteomics* .
- Hansen, K. D., Langmead, B. & Irizarry, R. A. (2012), ‘Bsmooth: from whole genome bisulfite sequencing reads to differentially methylated regions’, *Genome biology* **13**(10), R83.
- Hebestreit, K., Dugas, M. & Klein, H.-U. (2013), ‘Detection of significantly differentially methylated regions in targeted bisulfite sequencing data’, *Bioinformatics* **29**(13), 1647–1653.
- Irizarry, R. A., Ladd-Acosta, C., Carvalho, B., Wu, H., Brandenburg, S. A., Jeddelloh, J. A., Wen, B. & Feinberg, A. P. (2008), ‘Comprehensive high-throughput arrays for relative methylation (charm)’, *Genome research* **18**(5), 780–790.
- Irizarry, R. A., Ladd-Acosta, C., Wen, B., Wu, Z., Montano, C., Onyango, P., Cui, H., Gabo, K., Rongione, M., Webster, M. et al. (2009), ‘Genome-wide methylation analysis of human colon cancer reveals similar hypo-and hypermethylation at conserved tissue-specific cpg island shores’, *Nature genetics* **41**(2), 178.
- Ishwaran, H. & James, L. F. (2003), ‘Generalized weighted chinese restaurant processes for species sampling mixture models’, *Statist. Sinica* **13**, 1211–1235.

- Ishwaran, H. & Zarepour, M. (2002), ‘Dirichlet prior sieves in finite normal mixtures’, *Statistica Sinica* **12**, 941–963.
- Jaffe, A. E., Murakami, P., Lee, H., Leek, J. T., Fallin, M. D., Feinberg, A. P. & Irizarry, R. A. (2012), ‘Bump hunting to identify differentially methylated regions in epigenetic epidemiology studies’, *International journal of epidemiology* **41**(1), 200–209.
- Kim, M., Kim, J.-H., Baek, S.-J., Kim, S.-Y. & Kim, Y. S. (2016), ‘Specific expression and methylation of slit1, slit2, slit3, and mir-218 in gastric cancer subtypes’, *International journal of oncology* **48**(6), 2497–2507.
- Kim, S., Tadesse, M. G. & Vannucci, M. (2006), ‘Variable selection in clustering via dirichlet process mixture models’, *Biometrika* **93**, 877–893.
- Leek, J. T., Scharpf, R. B., Bravo, H. C., Simcha, D., Langmead, B., Johnson, W. E., Geman, D., Baggerly, K. & Irizarry, R. A. (2010), ‘Tackling the widespread and critical impact of batch effects in high-throughput data’, *Nature reviews. Genetics* **11**(10).
- Li, D., Wang, X., Lin, L. & Dey, D. K. (2016), ‘Flexible link functions in nonparametric binary regression with gaussian process priors’, *Biometrics* **72**(3), 707–719.
- Lijoi, A., Mena, R. & Prünster, I. (2007a), ‘Bayesian nonparametric estimation of the probability of discovering new species’, *Biometrika* **94**, 769–786.
- Lijoi, A., Mena, R. & Prünster, I. (2007b), ‘Controlling the reinforcement in bayesian nonparametric mixture models’, *Journal of the Royal Statistical Society: Series B (Statistical Methodology)* **69**, 715–740.
- Lijoi, A. & Prünster, I. (2010), *Models beyond the Dirichlet process*, Cambridge Series in Statistical and Probabilistic Mathematics, pp. 80–136.
- MacEachern, S. N. (1994), ‘Estimating normal means with a conjugate style dirichlet process prior’, *Communications in Statistics-Simulation and Computation* **23**(3), 727–741.
- Maekita, T., Nakazawa, K., Mihara, M., Nakajima, T., Yanaoka, K., Iguchi, M., Arii, K., Kaneda, A., Tsukamoto, T., Tatematsu, M. et al. (2006), ‘High levels of aberrant dna methylation in helicobacter pylori-infected gastric mucosae and its possible association with gastric cancer risk’, *Clinical Cancer Research* **12**(3), 989–995.
- Medvedovic, M., Yeung, K. Y. & Bumgarner, R. E. (2004), ‘Bayesian mixture model based clustering of replicated microarray data’, *Bioinformatics* **20**, 1222–1232.
- Müller, P. & Mitra, R. (2013), ‘Bayesian nonparametric inference—why and how’, *Bayesian analysis (Online)* **8**(2).
- Müller, P., Quintana, F. & Rosner, G. (2004), ‘A method for combining inference across related nonparametric bayesian models’, *Journal of the Royal Statistical Society, Series B* **66**, 735–749.
- Murphy, S. J., Hart, S. N., Lima, J. F., Kipp, B. R., Klebig, M., Winters, J. L., Szabo, C., Zhang, L., Eckloff, B. W., Petersen, G. M. et al. (2013), ‘Genetic alterations associated with progression from pancreatic intraepithelial neoplasia to invasive pancreatic tumor’, *Gastroenterology* **145**(5), 1098–1109.
- Network, C. G. A. R. et al. (2014), ‘Comprehensive molecular characterization of gastric adenocarcinoma’, *Nature* **513**(7517), 202.

- Newton, M. A., Noueiry, A., Sarkar, D. & Ahlquist, P. (2004), ‘Detecting differential gene expression with a semiparametric hierarchical mixture method’, *Biostatistics* **5**(2), 155–176.
- Park, Y., Figueroa, M. E., Rozek, L. S. & Sartor, M. A. (2014), ‘Methylsig: a whole genome dna methylation analysis pipeline’, *Bioinformatics* **30**(17), 2414–2422.
- Perman, M., Pitman, J. & Yor, M. (1992), ‘Size-biased sampling of poisson point processes and excursions’, *Probability Theory and Related Fields* **92**(1), 21–39.
- Rackham, O. J., Dellaportas, P., P. E. & Bottolo, L. (2015), ‘Wgbssuite: simulating whole-genome bisulphite sequencing data and benchmarking differential dna methylation analysis tools’, *Bioinformatics* **31**(14), 2371–2373.
- Rodriguez, A., B., D. D. & Gelfand, A. E. (2008), ‘The nested dirichlet process (with discussion)’, *Journal of the American Statistical Association* **103**, 1131–1144.
- Saito, Y., Tsuji, J. & Mituyama, T. (2014), ‘Bisulfighter: accurate detection of methylated cytosines and differentially methylated regions’, *Nucleic acids research* p. gkt1373.
- Sethuraman, J. (1994), ‘A constructive definition of dirichlet priors’, *Statistica sinica* pp. 639–650.
- Siegel, R. L., Miller, K. D. & Jemal, A. (2017), ‘Cancer statistics, 2017’, *CA: A Cancer Journal for Clinicians* **67**(1), 7–30.
- Song, Q., Decato, B., Hong, E. E., Zhou, M., Fang, F., Qu, J., Garvin, T., Kessler, M., Zhou, J. & Smith, A. D. (2013), ‘A reference methylome database and analysis pipeline to facilitate integrative and comparative epigenomics’, *PloS one* **8**(12), e81148.
- Subramaniam, S. & Hsiao, G. (2012), ‘Gene-expression measurement: variance-modeling considerations for robust data analysis’, *Nature immunology* **13**(3), 199–203.
- Sun, D., Xi, Y., Rodriguez, B., Park, H. J., Tong, P., Meong, M., Goodell, M. A. & Li, W. (2014), ‘Moabs: model based analysis of bisulfite sequencing data’, *Genome biology* **15**(2), R38.
- Tao, K., Wu, C., Wu, K., Li, W., Han, G., Shuai, X. & Wang, G. (2012), ‘Quantitative analysis of promoter methylation of the ednrb gene in gastric cancer’, *Medical Oncology* **29**(1), 107–112.
- Teh, Y. W., Jordan, M. I., Beal, M. J. & Blei, D. M. (2006), ‘Hierarchical dirichlet processes’, *J. Am. Statist. Ass.* **101**, 1566–1581.
- Tomlinson, G. & Escobar, M. (2003), ‘Analysis of densities’, *Talk given at the Joint Statistical Meeting* **103**, 1131–1144.
- Tsunoda, S., Smith, E., De Young, N. J., Wang, X., Tian, Z.-Q., Liu, J.-F., Jamieson, G. G. & Drew, P. A. (2009), ‘Methylation of cldn6, fbn2, rbp1, rbp4, tfpi2, and tmeff2 in esophageal squamous cell carcinoma’, *Oncology reports* **21**(4), 1067–1073.
- Vedeld, H. M., Goel, A. & Lind, G. E. (2017), Epigenetic biomarkers in gastrointestinal cancers: The current state and clinical perspectives, in ‘Seminars in cancer biology’, Elsevier.
- Vrana, D., Hlavac, V., Brynychova, V., Vaclavikova, R., Neoral, C., Vrba, J., Aujesky, R., Matzenauer, M., Melichar, B. & Soucek, P. (2018), ‘Abc transporters and their role in the neoadjuvant treatment of esophageal cancer’, *International journal of molecular sciences* **19**(3), 868.

- Wang, D., Yan, L., Hu, Q., Sucheston, L. E., Higgins, M. J., Ambrosone, C. B., Johnson, C. S., Smiraglia, D. J. & Liu, S. (2012), ‘Ima: an r package for high-throughput analysis of illumina’s 450k infinium methylation data’, *Bioinformatics* **28**(5), 729–730.
- Warden, C. D., Lee, H., Tompkins, J. D., Li, X., Wang, C., Riggs, A. D., Yu, H., Jove, R. & Yuan, Y.-C. (2013), ‘Cohcap: an integrative genomic pipeline for single-nucleotide resolution dna methylation analysis’, *Nucleic acids research* **41**(11), e117–e117.
- Yu, X. & Sun, S. (2016), ‘Hmm-dm: identifying differentially methylated regions using a hidden markov model’, *Statistical applications in genetics and molecular biology* **15**(1), 69–81.
- Zeger, S. L. & Karim, M. R. (1991), ‘Generalized linear models with random effects: A gibbs sampling approach’, *Journal of the American Statistical Association* **86**, 79–86.